

Toward Functional Biointerfaces with Origami-on-a-Chip

Alonso Ingar Romero, Qianru Jin, Kevin Kit Parker, Joe Alexander, Bernhard Wolfrum, and Tetsuhiko F. Teshima*

Studying the behavior of electroactive cells, such as firing dynamics and chemical secretion, is crucial for developing human disease models and therapeutics. Following the recent advances in cell culture technology, traditional monolayers are optimized to resemble more 3D, organ-like structures. The biological and electrochemical complexity of these structures requires devices with adaptive shapes and novel features, such as precise electrophysiological mapping and stimulation in the case of brain- and heart-derived tissues. However, conventional organ-on-chip platforms often fall short, as they do not recreate the native environment of the cells and lack the functional interfaces necessary for long-term monitoring. Origami-on-a-chip platforms offer a solution for this problem, as they can flexibly adapt to the structure of the desired biological sample and can be integrated with functional components enabled by chosen materials. In this review, the evolution of origami-on-a-chip biointerfaces is discussed, emphasizing folding stimuli, materials, and critical findings. In the prospects, microfluidic integration, functional tissue engineering scaffolds, and multi-organoid networks are included, allowing patient-specific diagnoses and therapies through computational and in vitro disease modeling.

1. Introduction

Computational models replicating the human body are promising in shaping future medicine.^[1] They can provide personalized diagnoses and therapeutic options without expensive and time-consuming tests. Importantly, they promise to predict disease course and patients' response to treatment.^[2] To develop such a model, there is a need for significant quantities of biological data from patients with multiple phenotypes and stages of

disease progression. Here, the goal is to identify relevant variables that affect a certain physiological behavior as well as how they influence each other. Building such a database is challenging from both ethical and medical perspectives, as it is not possible to isolate the behavior of single organs in a patient. Animal trials are also ethically disputable and often fail to accurately mirror human physiology. One increasingly popular approach to obtain the desired data is by using wearable sensors, as they are inexpensive and suitable for long-term recording. This approach allows only for indirect measurements of internal physiological parameters, making it heavily dependent on environmental factors and non-standardized validation procedures.^[3] Another emerging method to record data for disease modeling applications is tissue and organoid culture.^[4] By isolating distinct properties of individual organs as well as observing disease progression at early developmental stages, tissue and

organoid culture offer promising avenues to tackle the aforementioned challenges. In addition, facilitating direct and long-term monitoring of multiple physiological parameters from these samples to feed future computational models requires the development of functional biointerfaces. The combination of organoid technology with functional biointerfaces not only aids in understanding disease mechanisms at a cellular level but also contributes to the refinement and validation of computational models, thereby enhancing their predictive power and clinical relevance.


A. Ingar Romero, B. Wolfrum, T. F. Teshima
Neuroelectronics
Munich Institute of Biomedical Engineering
Department of Electrical Engineering
TUM School of Computation
Information and Technology
Technical University of Munich
Hans-Piloty-Strasse 1, 85748 Garching, Germany
E-mail: tetsuhiko.teshima@ntt-research.com

A. Ingar Romero, J. Alexander, B. Wolfrum, T. F. Teshima
Medical & Health Informatics Laboratories
NTT Research Incorporated
940 Stewart Dr., Sunnyvale, CA 94085, USA

Q. Jin, K. K. Parker
Disease Biophysics Group
Harvard John A. Paulson School of Engineering and Applied Sciences
Harvard University
Science and Engineering Complex, 150 Western Ave., Boston,
MA 02134, USA

K. K. Parker
Wyss Institute for Biologically Inspired Engineering
Harvard University
201 Brookline Ave., Boston, MA 02115, USA

T. F. Teshima
Department of Mechanical Engineering
Keio University
Hiyoshi, Kohoku-ku, Yokohama 223-8522, Japan

 The ORCID identification number(s) for the author(s) of this article can be found under <https://doi.org/10.1002/aisy.202400055>.

© 2024 The Author(s). Advanced Intelligent Systems published by Wiley-VCH GmbH. This is an open access article under the terms of the Creative Commons Attribution License, which permits use, distribution and reproduction in any medium, provided the original work is properly cited.

DOI: 10.1002/aisy.202400055

The past decade has witnessed a revolution in cell culture technology, moving from traditional monolayer culture to organ-like, organized 3D culture, also known as organoids.^[5] Combined with the discovery of the programmability of mature cells into pluripotent cells,^[6] researchers are now able to model human development and diseases in a dish in a way closer to what occurs in vivo. Not only does this reduce the need for animal testing, whose applicability to humans and ethical implications are highly debated, but it also offers the possibility of obtaining patient-specific data in a fast, efficient, and high-throughput fashion. For example, human-induced pluripotent stem cells (hiPSC) derived from the skin could represent the genetic background and disease mutation.^[7] Several genetic diseases have been successfully modeled using organoids in recent years. These include cystic fibrosis,^[8] hereditary multiple intestinal atresia,^[9] alagille syndrome,^[10] and microcephaly.^[11] Some studies have also shown that organoids are promising candidates to model neurodegenerative diseases such as Alzheimer's^[12] and Parkinson's disease.^[13] Moreover, organoids derived from mouse or human tumors have been used to study different types of cancer, such as colorectal cancer,^[14] liver cancer,^[15] and breast cancer.^[16] A full review covering the recent progress of organoids in disease modeling and other applications can be found in a previous article.^[4]

Conventionally, organoids form 3D structures spontaneously on top of or inside their extracellular matrix (ECM) materials, resulting in uncontrollable final shapes. In contrast, engineered 3D scaffolds provide extracellular microenvironments that mimic hierarchical tissue structures within spatially confined physiological environments. Both organoids and engineered 3D tissues have been used in microphysiological systems or organs-on-chips for disease modeling and high-fidelity studies of physiology because both aspire to mimic enough of the cellular microenvironment to recapitulate both the physiology and pathophysiology of interest. However, engineered tissues play the more critical role within the pharma industry because of the higher repeatability. Especially, genetic diseases such as inherited cardiomyopathies^[17] and Duchenne's muscular dystrophy^[18] have been successfully modeled in microphysiological systems with controlled tissue geometries. The parameter space in engineered tissues is constrained by design of the tissues and cell populations.^[19] On the contrary, the self-organization process in organoids does not necessarily include all the spatial and temporal cues nor cell demographics and chemistry, of the organ of interest. For these reasons, organs-on-chips based on engineered tissues are more amenable to computational modeling.

Most of the reported disease models using organoids and engineered tissues are evaluated using microscopy techniques. While this is sufficient for the visualization of important biomarkers such as protein expression and cellular morphology, to be able to use the obtained data for computational models requires the recording of digital biomarkers through the incorporation of biosensors into the culture platforms. In this context, electrophysiological properties such as action potentials, field potentials, and synaptic activity are especially relevant, as they can serve as biomarkers for neuronal or cardiac function. In addition to their relevance for clinical diagnosis, electrical signals can also be used to stimulate electrically active organs for treating several diseases. Some examples include arrhythmias,^[20] heart

failure,^[21] peri-/myocarditis,^[22] Tourette disorder,^[23] epilepsy,^[24] and hemiparesis.^[25] Electrical connections are also necessary for evaluating other critical physiological parameters from integrated sensors, such as temperature, pH, and mechanical activity.^[26] Thus, the successful modeling of diseases and treatments in vitro requires the integration of electrical interconnects into the respective culture platforms. However, conventional multiwell plates and organ-on-chip platforms mainly allow for optical analysis, which, despite essential, falls short for long-term monitoring due to potential phototoxicity.^[27] They also lack the ability to electrically stimulate samples and the high time resolution required for recording fast cell firing signals. Traditional planar microelectrode arrays (MEAs) are unsuitable for interfacing 3D structures, as they are rigid and provide limited contact. Pillars have been built into these MEAs,^[28] potentially allowing for internal electrophysiological measurements within cell assemblies.^[29] However, the applied mechanical force may lead to tissue damage. Hence, there is a need for flexible, ultrasoft, conformal structures, which precisely guide the tissue growth into a desired shape while also including electrical interfaces and other biosensors to monitor relevant physiological parameters. In this context, origami-on-a-chip technology offers a compelling solution, as it offers the possibility to fabricate complex-shaped scaffolds with minimal damage to the cultured tissue as well as to easily integrate multifunctional components by using conventional, planar microfabrication techniques. The combination with 3D cell culture further facilitates high-density multiparametric physiological mapping and stimulation, which are especially relevant in both basic and clinical cardiology.^[26]

Origami-on-a-chip involves transforming flat, 2D structures into intricate 3D configurations.^[30] This technology merges the advantages of planar microfabrication with the versatility of 3D interfacing. Compared with 3D printing, planar microfabrication has higher resolution, robustness, and stability. In combination with ECM, 3D self-folding structures can be used as scaffolds to guide cell growth and aggregation into complex shapes. They are optimal for sensing purposes, as they provide a conformal and tight contact with the biological sample, which maximizes the signal-to-noise ratio. The conformation is also crucial for organoid culture since they attach only partially to planar substrates, making it difficult to investigate spatiotemporal electrophysiological behavior. Atomic force microscope-like manipulation with a soft polydimethylsiloxane (PDMS) probe may improve organoid-sensor contact but is still limited to a small area and potentially increases mechanical stress to the sample.^[31] For these reasons, self-folding devices have made advances in the fields of tissue engineering, single-cell, and organoid analysis. In the following, the terms origami, self-folding, and self-assembly will be treated interchangeably.

Since the first rolled-up tubes on a chip were reported,^[32] several self-assembly approaches have been demonstrated for cell culture applications (**Table 1**). With the advances in organoid technology, some origami-on-a-chip platforms have been developed to interact with these larger and more complex 3D structures. The platforms enable encapsulation and sensing functionalities, such as electrical, thermal, chemical, and optical sensing. A further advantage of origami-on-a-chip is that the complex 3D shapes achievable via self-folding can serve as scaffolds to grow more geometrically complex cell assemblies, such

Table 1. The 3D self-assembled devices reported for biological applications in the past two decades and their characteristics.

Stress-driving materials	Sacrificial layer	Shape	Feature size	Folding stimulus	Sample type	References
Cu/Cr/photoresist trilayer	PVA	Box	50–500 μm	Temperature change	L929 fibroblasts, crustacean Triops, Artemia eggs	[34b]
Au/Cr bilayer	Cu	Cylinders, spirals, and bidirectionally folded sheets	$\approx 500 \mu\text{m}$ (estimated from figures)	Spontaneous	L929 mouse fibroblasts	[38b]
SiO/SiO ₂ bilayer	ARP-3510 photoresist	Tube	4–18 μm	Spontaneous	Yeast, embryonic fibroblast mouse cells, mitotic mammalian cells	[59]
PCL/poly(NIPAM) bilayer	None	Gripper	$\approx 200 \mu\text{m}$ (estimated from figures)	Temperature change	Yeast	[34c]
Si/SiGe bilayer	SiO ₂	Tube	4–8.2 μm	Spontaneous	Neurites	[41]
PSI/PCL bilayer	None	Tube	18–100 μm	Swelling	Yeast	[49]
Differentially strained PDMS bilayer	None	Tube	100–2000 μm	Shrinking	HUVECs, SMCs, NIH/3T3	[36b]
Cells adhered to a parylene plate coated with fibronectin	Gelatin	Tube, box	$\approx 50\text{--}100 \mu\text{m}$	Shrinking	NIH/3T3, BAOSMCs, BCAECs, HUVECs, primary rat cardiomyocytes (CMs)	[55]
p(NIPAM-AA-BA)/p(MMA-BA) bilayer	None	Aggregated tubes	$\approx 20 \mu\text{m}$	Swelling	Yeast	[37c]
PEG-based hydrogel bilayer	None	Spheres, helices, tubes	$\approx 100\text{--}1200 \mu\text{m}$	Swelling	β -TC-6 cells	[50]
GaAs/InGaAs bilayer	AlAs	Tube	2–5 μm	Spontaneous	Neurites	[42]
Gelatin/copolymer of hexanediol and fumaryl chloride (PHF-Q)C bilayer	None	Tube	10–20 μm	Temperature change	neural stem cells	[34e]
SiO/SiO ₂ bilayer	Cu/Ge	Gripper, tube	10–300 μm	Spontaneous	Mouse fibroblasts, red blood cells, neonatal rat ventricular CMs, MDA-MB-231 breast cancer cells, HPMECs, VSMCs	[34a,40,43]
Silicon nitride (SiNx) film	Si (111), Ge	Tube	$\approx 2.7\text{--}4.4 \mu\text{m}$	Spontaneous	Neurites	[38a]
Crystalline silicon nanomembrane over PDMS substrate	None	Buckle-delaminated channels	3.5 μm	Shrinking	Neurites	[36a,53]
PCL/gelatin bilayer	None	Tube	$\approx 130 \mu\text{m}$ (estimated from figures)	Temperature change	Yeast	[34d]
Various bimetallic or oxide layers	Cu	Tube	15–225 μm	Spontaneous	Endothelial cells, astrocytes	[60]
Graphene/PD/poly(NIPAM) trilayer	Al	Gripper	60 μm	Temperature change	Live breast cancer cells	[34f]
Silk/parylene bilayer	Ca–alginate	Tube	40–80 μm	Swelling	Chinese Hamster Ovary (CHO) cells, Human embryonic kidney 293 (HEK) cells, cardiomyocytes, neural cells.	[37a]
Mouse embryonic fibroblast (MEF) clusters in ECM	None	Tube, helix, sphere, cube, tessellation	400–550 μm	Shrinking	MEFs, Caco-2, HUVECs	[56]
p(OEGMA-DSDMA)/P(AAm-BAC) bilayer	Na–alginate	Gripper	4 mm	Temperature change	Human telomerase reverse transcriptase ⁺ human aortic endothelial cells (hTERT HAEC)	[47]

Table 1. Continued.

Stress-driving materials	Sacrificial layer	Shape	Feature size	Folding stimulus	Sample type	References
Graphene/parylene bilayer	Ca–alginate	Tube	10–100 μm	Spontaneous	Neurons, HUVECs, Human umbilical artery smooth muscle cells (HUASMCs)	[45a,c,d, 61a]
Metal/polymer multilayer	Ge	Tube	$\approx 160 \mu\text{m}$	Spontaneous	Stem-cell-derived cardiac spheroids	[38c]
SiO/SiO ₂ bilayer + paraffin wax layer	None	Gripper	15 μm	Temperature change	MDA-MB-231 cells	[48]
Multilayer stack over pre-strained PDMS substrate	None	Pouch-shaped “cage”	480–600 μm	Shrinking	Cortical spheroids	[54]
Differentially cross-linked SU-8 bilayer/gradient layer	Ge	Gripper	400–600 μm	Swelling	hiPSCs-derived brain organoids	[51]

as ventricular structures, which are essential to mimic the behavior of the human heart.^[33]

2. Development of Self-Folding Biointerfaces

Origami, or the folding process, is driven by differences in material deformation in the multilayered constructs. Different mechanisms have been developed to ensure highly parallel and reproducible folding, with most utilizing strain mismatch between layers of materials. The differences in material deformation have been generated by thermal expansion (Figure 1A),^[34] magnetic forces (Figure 1B),^[35] shrinking (Figure 1C),^[36] swelling (Figure 1D),^[37,49] or adjusting the deposition process (Figure 1E).^[38]

In the case of organoids, it is generally necessary to wait for the spontaneous forming of 3D structures, which requires a stochastic symmetry break. On the contrary, engineered tissues enable the shape forming to be programmed and can replicate a tissue with dimensional precision and repeatability.^[39] One important design goal for origami devices is to obtain free-standing structures, which requires dissolving a sacrificial layer. Photolithography is a powerful approach, as it allows patterning the sacrificial layer for selective folding. An un-patterned sacrificial layer allows complete release of self-folding structures, which is helpful for surgical and implantation purposes (Figure 2A).^[34a,40] Patterned sacrificial layers allow the 3D devices to be partially attached to the substrate for stable observation and electrical interfacing (Figure 2B).^[38c] By sacrificial layer patterning, lithography-based self-folding devices could be designed as in vitro analysis platforms. In principle, any material that can be dissolved or etched is a candidate for the sacrificial layer underneath the foldable layers. However, interfacing with living organisms demands specific material selection and folding mechanisms. For example, the chosen materials must demonstrate long-term stability and biocompatibility. The dissolution of the sacrificial layer should also have low toxicity to enable cell seeding before encapsulation. Finally, appropriate temperature and pH ranges for the cell culture environment should be maintained.

Despite the challenges mentioned earlier, researchers have reported several approaches for biocompatible self-folding

devices in the past decade. Here, we categorized the methods based on their folding stimulus, sacrificial layer materials, and the integrations of additional functionalities such as electrical, optical, and magnetic sensing. Other important design factors include structure size and sample type, depending on their targeted applications in individual or larger cell aggregates.

2.1. Folding Mechanisms and Stimulation

The most common method to induce folding is the dissolution of a sacrificial layer under an intrinsically stressed structure. The internal stress can be generated by combining two epitaxially grown material layers with different lattice constants. During deposition, the second layer will be mechanically strained to match the lattice constant of the first layer. After being released, the materials tend to relax toward their bulk lattice constants by rolling up. Examples of this approach include bilayers of Si/SiGe^[41] and GaAs/InGaAs.^[42] Another method is based on a SiO/SiO₂ bilayer deposited via electron beam evaporation (Figure 2C,D). Here, the intrinsic stress is generated due to differences in thermal expansion during evaporation and can be controlled by tuning the parameters of the deposition process.^[43] It has been shown that varying the plasma frequency and the temperature during the plasma-enhanced chemical vapor deposition of a single silicon nitride layer can also induce the necessary stress to create self-folding tubes. An advantage of this approach is its compatibility with a broad range of substrates and biocompatible sacrificial layers.^[38a] Intrinsic stress can also be induced in polymeric materials such as parylene C during chemical vapor deposition and annealing.^[44] Combining it with a more temperature-stable material such as graphene thus leads to rolling upon release from the substrate.^[45]

Temperature control is another strategy to stimulate self-folding. For temperature-triggered folding of a bilayer, one layer would undergo deformation with temperature change while the other remains undeformed. For example, researchers have reported a bilayer composed of a biodegradable hydrophobic polycaprolactone layer (PCL) and a thermoresponsive poly-(N-isopropylacrylamide) copolymer with 1 mol% 4-acryloylbenzophenone comonomer (poly(NIPAM-ABP)) layer.^[34c] The structures started to curl and formed tubes when the

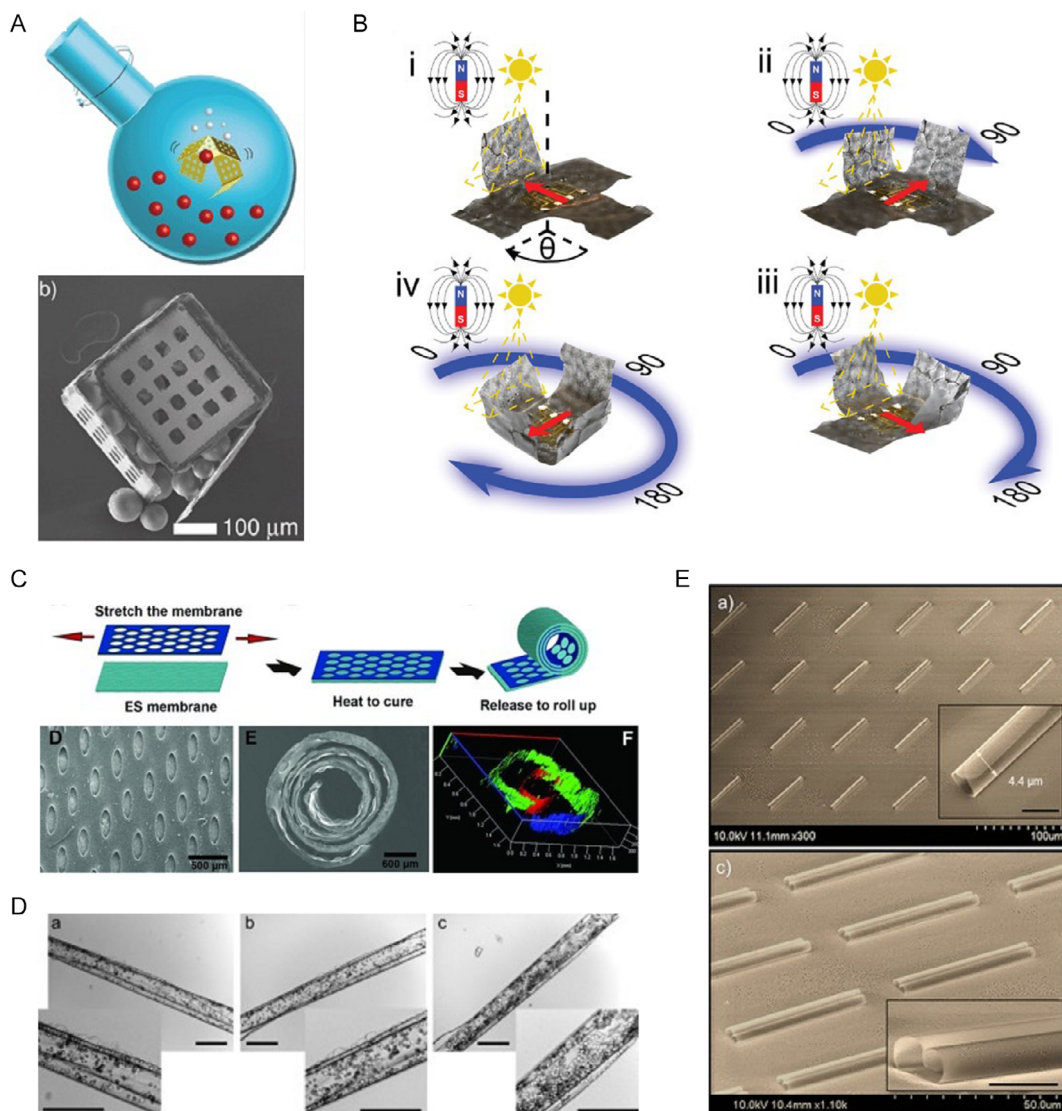


Figure 1. Methods to create general-purpose self-folding devices. A) Schematic illustration and scanning electron microscope (SEM) image of an untethered microcontainer irreversibly folded via temperature change loaded with glass beads. B) Assembly steps of magnetic origami structures with an external magnetic field. C) Fabrication of a tubular structure by using the shrinking force of a pre-stretched PDMS layer upon relaxation. D) PSI/PCL micro-roll assembled due to the hydrolyzation of PSI, which produces a biodegradable water-swellaible polymer. The image sequence shows the encapsulation of yeast cells. Scale bar is 100 μm . E) SEM images of SiNx microtube arrays formed after sacrificial layer etching due to internal stress generated during the deposition process. (A) Reproduced with permission.^[34b] Copyright 2008, Royal Society of Chemistry. (B) Reproduced under the terms of the Creative Commons CC BY license.^[35] Copyright 2021, The Author(s). Advanced Materials published by Wiley-VCH GmbH. (C) Reproduced with permission.^[36b] Copyright 2012, WILEY-VCH Verlag GmbH & Co. KGaA, Weinheim. (D) Reproduced with permission.^[49] Copyright 2011, American Chemical Society. (E) Reproduced with permission.^[38a] Copyright 2014, American Chemical Society.

temperature decreased below the low critical solution temperature of poly(NIPAM-ABP) at 28 °C. Elevating the temperature leads to complete unrolling of the tubes (**Figure 3A**). Gelatin has also been demonstrated as active component, due to its biodegradable and temperature-dependent swelling properties (**Figure 3B**).^[34d] Box-shaped microcontainers were shown to fold upon heating to 40 °C, a temperature low enough to provide a stable environment for some living cells.^[34b] The authors designed the hinge with a trilayer of chromium, copper, and photoresist for this structure. When the photoresist softened

with temperature rise, the intrinsic tension generated during the chromium deposition process drives the folding.^[46] Further thermoresponsive materials include a graphene/polydopamine/poly(NIPAM) trilayer,^[34f] poly(oligoethylene glycol methyl ether methacrylate-bis(2-methacryloyl)oxyethyl disulfide) (p(OEGMA-DSDMA)),^[47] and thermosensitive paraffin wax^[48] to induce self-folding (**Figure 3C**).

Another commonly used self-assembly method is based on combining materials with swelling properties and rigid materials, such as a silk fibroin protein and parylene C.^[37a] Here, the

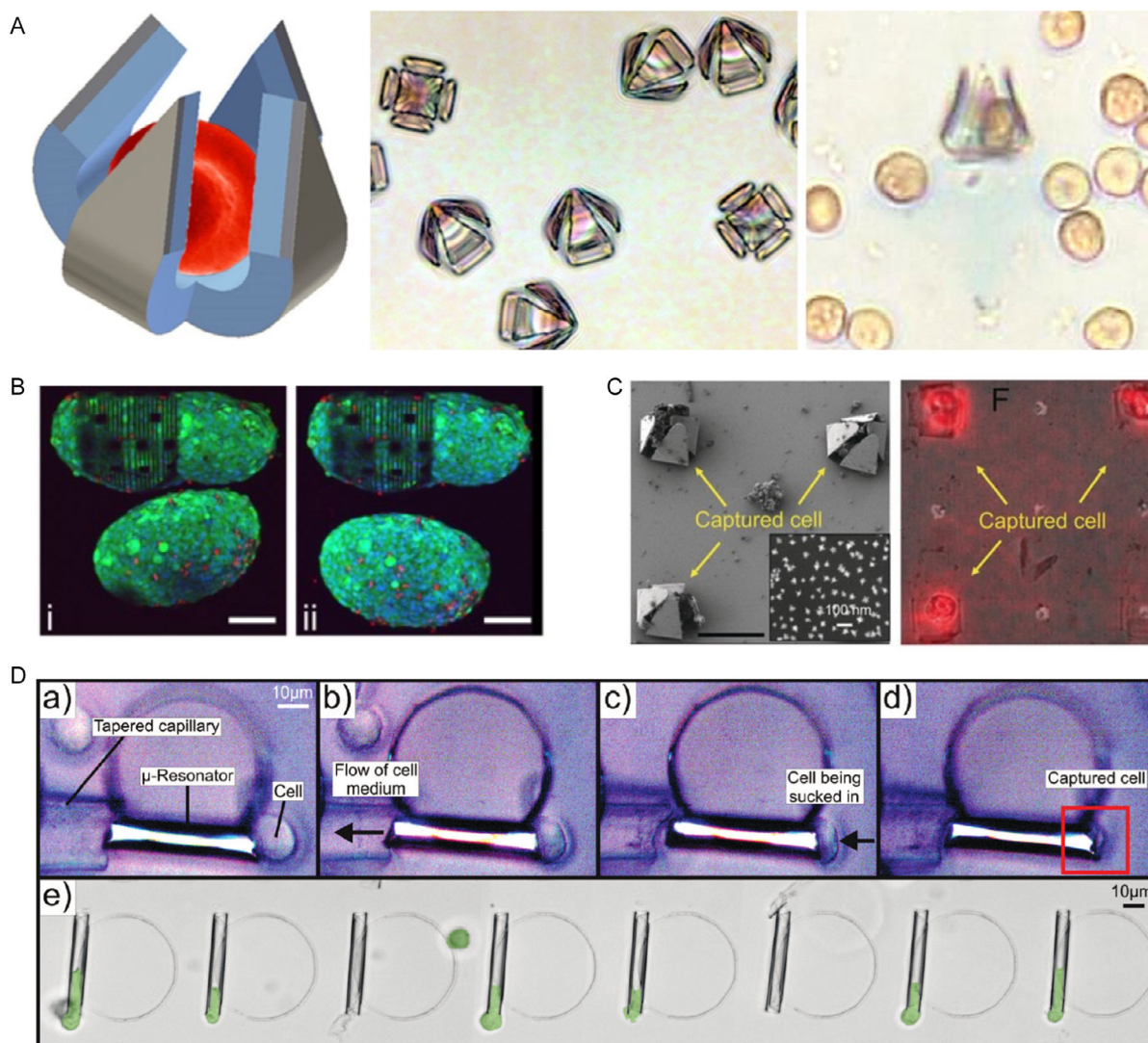


Figure 2. Encapsulation of single cells and cell aggregates inside spontaneously folded structures upon the dissolution of a sacrificial layer. A) Left: illustration of an untethered single-cell gripper with a captured red blood cell. Middle: optical images of single-cell grippers after closing. Right: red blood cell trapped inside a gripper. B) Live/dead assay performed on encapsulated (top) and nonencapsulated (bottom) cardiac spheroids, imaged immediately after encapsulation (left) and after 1 h (right). C) Left: SEM image of the gold nanostar (GNS) coating inside the microgripper surface. Right: overlaid SERS and optical image of trapped cells in GNS-modified microgrippers. D) Image sequence of a mouse embryonic fibroblast cell (NIH/3T3) being inserted into a microtube resonator for detection. (A) Reproduced with permission.^[40] Copyright 2014, American Chemical Society. (B) Reproduced under the terms of the Creative Commons CC BY license.^[38c] Copyright 2019, The Author(s). Published by American Association for the Advancement of Science. (C) Reproduced with permission.^[34a] Copyright 2017, Wiley-VCH Verlag GmbH & Co. KGaA, Weinheim. (D) Reproduced with permission.^[59b] Copyright 2011, American Chemical Society.

micro-rolls fold upon immersion in a fluid such as cell culture medium (Figure 3D). A system of self-folding tubes consisting of a p(NIPAM-AA-BPA)/p(MMA-BA) bilayer has also been assembled via pH-dependent swelling in an aqueous environment.^[37c] Another reported material combination is polysuccinimide (PSI) and PCL. Here, the water-swellaible properties of PSI emerge from its hydrolyzation in a physiological buffer environment.^[49] Further swelling-based approaches involve polyethylene glycol (PEG)-based hydrogels with different molecular weights^[50] (Figure 3E) and differentially cross-linked negative photo-resists, SU-8 (Figure 3F).^[51] One advantage of the latter method is that it

allows reversible folding via solvent exchange between acetone and water, making it suitable for robotic applications.^[52]

Finally, several research groups have reported self-folding devices based on the shrinking of a flexible material after it is released from a mechanically stretched state. For example, buckle-delaminated microchannels were developed by depositing a crystalline-silicon nanomembrane over a PDMS substrate. The combination was subsequently swollen using a solvent. Finally, solvent evaporation led to a compressive strain in the Si nanomembrane for channel formation (Figure 3G).^[36a,53] Similarly, researchers have used a mechanically pre-stretched

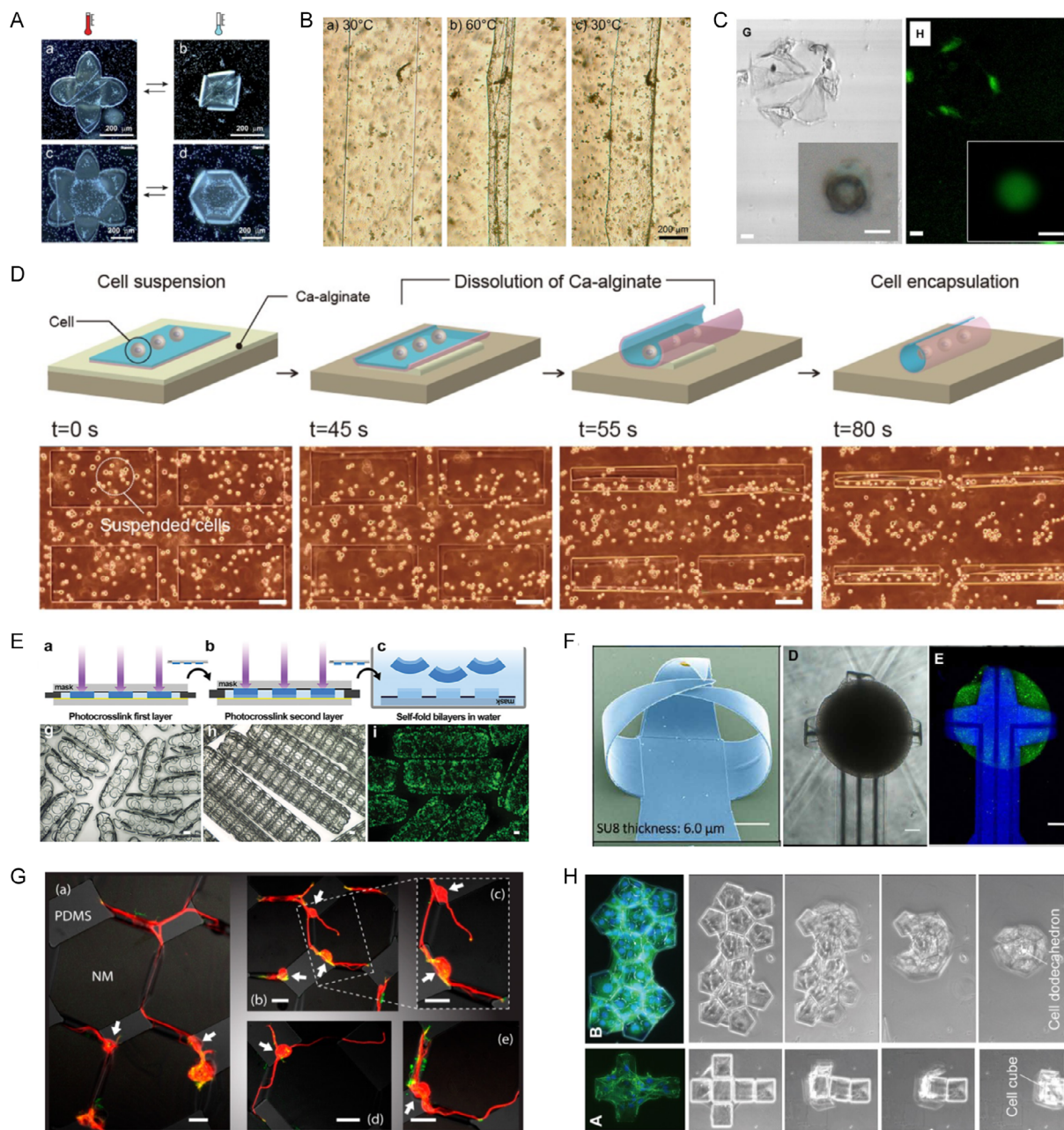


Figure 3. Biological samples trapped inside origami-on-a-chip platforms assembled via external stimuli. A) Reversible thermoresponsive PCL/poly(NIPAM) gripper encapsulating yeast cells (dark field microscopy). B) Temperature-triggered encapsulation and release of yeast cells inside PCL–gelatin tubes. C) Bright-field and fluorescence image of a live breast cancer cell encapsulated inside a functionalized graphene gripper. Scale bars: 10 μm . D) Time-lapse schematic and optical images illustrating mammalian cell encapsulation within silk/parylene microtubes. Scale bars: 100 μm . E) Top: fabrication steps of swellable structures based on differentially photo-cross-linked PEG bilayers. Bottom: bright-field images of cylindrical hydrogels with micropatterned holes and fluorescence image of cylinders with photo-encapsulated fibroblasts labeled with calcein (green). Scale bars: 200 μm . F) SEM (right), bright-field (middle), and confocal (right) images of 3D shell electrodes encapsulating brain organoids in a 3D shell microelectrode array (MEA). Scale bars: 100 μm . G) Top: confocal fluorescence microscope images showing guidance of neuronal outgrowths by buckle-delaminated channels while excluding the neuronal cell body (indicated by arrows). Bottom: 3D rendering of confocal images. Scale bars: 20 μm . H) Sequential images of cell-laden regular tetragon (left), regular dodecahedron (middle), and cylindrical tube (right) self-folded by cell traction force. (A) Reproduced with permission.^[34c] Copyright 2011, Royal Society of Chemistry. (B) Reproduced with permission.^[34d] Copyright 2015, American Chemical Society. (C) Reproduced under the terms of the Creative Commons CC BY license.^[34] Copyright 2017, The Author(s). Published by American Association for the Advancement of Science. (D) Reproduced under the terms of the Creative Commons CC BY license.^[37a] Copyright 2017, The Author(s). Published by Springer Nature Limited. (E) Reproduced with permission.^[50] Copyright 2013, WILEY-VCH Verlag GmbH & Co. KGaA, Weinheim. (F) Reproduced under the terms of the Creative Commons CC BY license.^[51] Copyright 2022, The Author(s). Published by American Association for the Advancement of Science. (G) Reproduced with permission.^[36a] Copyright 2014, American Chemical Society. (H) Reproduced under the terms of the Creative Commons CC BY license.^[55] Copyright 2012. The Author(s). Published by PLOS.

PDMS layer to induce the folding of adhered structures upon relaxation.^[36b,54] Another mechanism for shrinking-driven folding is based on cellular intrinsic traction forces.^[55] In this case, cells adhered to parylene microplates coated with fibronectin (Figure 3H). Upon dissolution of a sacrificial layer, the cells generated a traction force, which led to the self-assembly of different 3D structures. Mechanical compaction of the ECM during mesenchymal condensation can also lead to tissue folding via cell traction forces.^[56]

It is important to note that most of the folding mechanisms mentioned earlier do not happen in the Cartesian coordinates. The final self-folded 3D origami structures include not only the formation of cylindrical tubes but also spheroids with high sphericity or oblate spheroids. This is important since most biological tissues, when expanding the spatial scale of measurement, are a lopsided form of cylindrical or spheroid coordinates.^[57]

2.2. Materials for the Sacrificial Layer

One important design goal for origami devices is to obtain free-standing structures, which require dissolving a sacrificial layer. Just before dissolving a sacrificial layer, photolithographically engineered scaffold patterns possess an internal stress. Then, the removal of the sacrificial layer induces a deformation derived from the internal stress to a free-standing structure, which allows the programming of the folding time as well as many degrees of freedom to fold. However, it is important that the release of the engineered tissues from the abiotic substrate does not compromise the structural integrity of the tissue.^[58] A sacrificial layer can be created using positive photoresist, which can be easily removed by acetone to release the pre-strained layers.^[59] A SiO₂ layer can also be applied,^[41] as it can be etched using hydrofluoric acid. Other groups have reported sacrificial layers made of semiconductors like silicon and germanium,^[34a,38a,c,51] which could be dissolved by KOH and H₂O₂, respectively. Cu or Cr is a commonly used metal layer since it can be removed by FeCl₃^[38b] or chromium etchant.^[60]

One disadvantage of the approaches mentioned earlier is that the dissolution process is toxic for living organisms. In such cases, cells could only be cultured after the structures have folded. This reduces the success of encapsulation and limits the potential to guide and control the growth of the cells in the scaffolds, an essential feature for tissue engineering applications. Even though some authors have managed to seed cells before the copper sacrificial layer is fully etched,^[43a] meticulous work is required to prevent contact between the cells and the copper ions. In the case of larger cell spheroids, a micromanipulator is needed to open the structures prior to encapsulation.^[38c]

Some research groups have provided biocompatible materials and processes for structure release. One example is poly(vinyl alcohol), a water-soluble and biocompatible synthetic polymer. Gelatin is another material explored as a biocompatible sacrificial layer, as it can be dissolved when heated up to 37 °C.^[53] Researchers have also reported a calcium alginate sacrificial layer, which can be quickly dissolved by EDTA solution. As long as the EDTA concentration remains low, biological samples can be seeded safely before the dissolution process.^[37a,45c,d,61]

A further advantage of this method is that the structures fold after some minutes of applying the EDTA solution, in contrast with conventional etching methods, which takes hours.^[40]

Self-assembly approaches that use other kinds of folding stimuli like temperature change or swelling usually do not require the dissolution of a sacrificial layer and thus allow for encapsulation before or during the folding process.^[34c,37c,49] However, these field-stimulated mechanisms usually do not allow for partial detachment, which is achieved through selective etching or patterning of the sacrificial layer in the desired situation. One solution to this problem involves selective temperature-triggered folding via directed heating of prestressed hinges using low-power, commercial lasers.^[62]

2.3. Functional Materials

Until now, we mainly focused on material properties for structure-building purposes. In the case of analysis platforms, providing more advanced, label-free functionalities is necessary to automate and increase the amount of data that can be recorded at a time. For example, Schmidt and coworkers integrated optical microcavity resonators^[63] into their cell encapsulation devices by coating SiO/SiO₂ bilayer tubes with ferroelectric Hafnium(IV) oxide (HfO₂).^[59b] The tubes were then successfully applied to detect the presence of individual mouse embryonic fibroblast cells by measuring shifts in whispering gallery modes.

Magnetic stimulation is used for folding actuation and micro-robot locomotion to effectively manipulate encapsulated samples. Ionov and coworkers added Fe₃O₄ nanoparticles into their thermoresponsive microtubes.^[37b] Schmidt and collaborators used magnetic microtubes^[64] and helical structures^[65] made of magnetic materials to guide immotile single sperm cells in vitro via an external magnetic field (Figure 4A). This approach could lead to an effective therapy for male infertility due to poor sperm motility. Gracias and coworkers also incorporated magnetic materials into microgrippers to enable remote guidance through narrow conduits and fixed tissue sections ex vivo with an external magnetic field,^[47,48] making their devices potentially applicable in surgery and biopsy (Figure 4B).

Integrating electrically conductive materials into a self-foldable platform is necessary for recording and stimulating electrically active cells like cardiomyocytes or neurons. Compared to optical methods such as calcium imaging, electrical recording exhibits a superior temporal resolution and protects the samples from cell damage due to prolonged light exposure. Furthermore, electrical connections are imperative for obtaining digital data from multiple sensors for computational modeling purposes. Apart from this, electrical stimulation has been shown to play an important role in the culture of electroactive cells such as hiPSC-derived cardiomyocytes,^[66] which makes electrodes relevant for tissue engineering applications, by improving the maturity of stem cells. Even though traditional 2D MEAs can achieve this purpose, self-folding devices have shown to provide better signal qualities due to their close contact and better sealing (Figure 4C),^[61a] as well of the possibility for high density 3D mapping.^[38c] However, electrode integration into self-folding structures comes with several challenges. First, the most common conductive materials are metals, which are not stretchable.

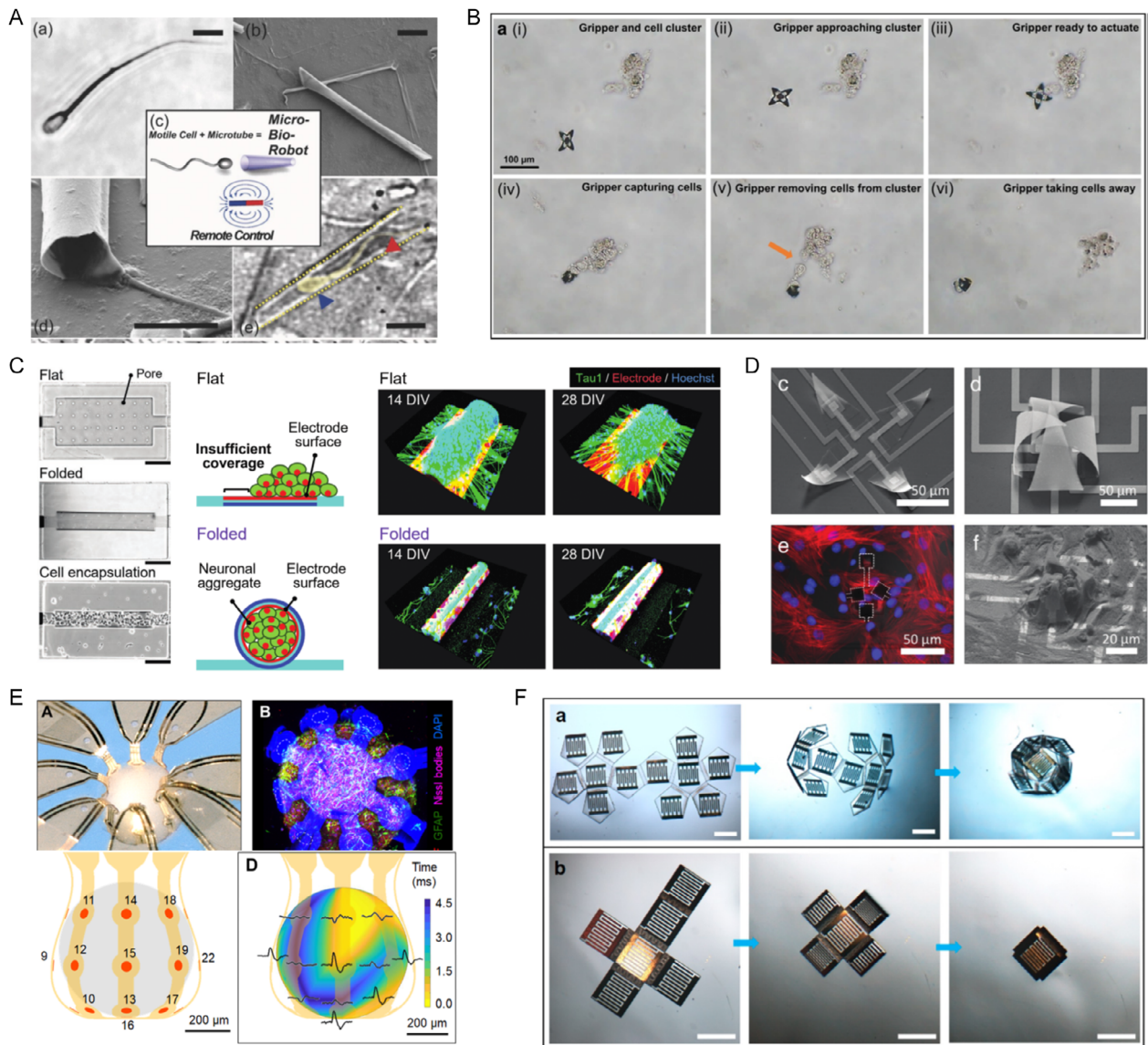


Figure 4. Self-folding devices with added magnetic, electrical, and optical functions. A) Optical, SEM, and schematic images of motile sperm cell trapped inside a rolled-up microtube with an incorporated magnetic layer for remote control. The blue arrow points at the sperm head, the red arrow points at the sperm flagella. All scale bars are 10 μm except for the bottom bar (50 μm). B) Process of an untethered gripper capturing and excising cells from a cell cluster. The gripper was guided by a magnetic field and actuated upon temperature increase. C) Left: phase-contrast images of flat and folded graphene-based electrodes before and after neuronal cell encapsulation. Scale bars represent 100 μm . Middle: schematic illustrations of cell–electrode interface in flat and folded states. Right: 3D reconstructed images of neuronal cell aggregates cultured on the flat and folded electrode. D) Top: SEM images of an individually addressable, multielectrode self-folding shell. Bottom: confocal fluorescence microscopy image of captured cardiomyocytes within electrode shells showing actin filaments (red) and cell nuclei (blue) with three electrodes wrapping around the cells (dashed white lines) and SEM picture of captured cardiomyocytes after fixation. E) Top left: optical image of a cortical spheroid enclosed in a pouch-shaped framework designed for electrophysiological recording. Top right: confocal microscope image of the spheroid in a similar structure without microelectrodes or interconnections. Bottom: schematic illustration of the microelectrodes' positions across the spheroid's surface and 3D plot of time latency associated with recorded field potentials. F) Self-folding process of hinged 3D $\text{MoS}_2\text{-Au-SU-8}$ photodetectors with interdigitated electrodes of different shapes. Scale bars are 1 mm. (A) Reproduced with permission.^[64] Copyright 2013, WILEY-VCH Verlag GmbH & Co. KGaA, Weinheim. (B) Reproduced with permission.^[48] Copyright 2020, American Chemical Society. (C) Reproduced under the terms of the Creative Commons CC BY license.^[61a] Copyright 2023, The Author(s). Advanced Functional Materials published by Wiley-VCH GmbH. (D) Reproduced under the terms of the Creative Commons CC BY license.^[43a] Copyright 2018, The Author(s). Published by WILEY-VCH Verlag GmbH & Co. KGaA, Weinheim. (E) Reproduced under the terms of the Creative Commons CC BY license.^[54] Copyright 2021, The Author(s). Published by American Association for the Advancement of Science. (F) Reproduced with permission.^[71] Copyright 2019, American Chemical Society.

Exposing them to strain can thus damage their conductivity, and one must implement special strategies such as microcracking to avoid this damage.^[67] Second, precise and localized electrical mapping is often crucial because several cardiac and neuronal diseases are linked to action potential propagation.^[68] For electrical mapping, the electrodes need to be exposed only in particular areas, and wholly passivated in the rest of the surface, which adds a layer of complexity to the fabrication process. Thus, high-quality dielectric materials with appropriate adhesion to the metal layers must be integrated into the self-folding structures. Finally, there are limitations regarding the maximum number of channels per device and the connection possibilities with amplifiers and other data processing hardware.

Despite the aforementioned challenges, plenty of materials have been tested as bioelectronic interfaces, including metals (Figure 4D),^[38c,43a,51,54,69] conducting polymers,^[51,59a] and carbon-based materials.^[61a,70] For self-folding devices, gold remains the most common material for the cell-electrode interface due to its inertness and high conductivity. A chromium layer was often used to improve the adhesion to the substrate (Figure 4E).^[54] In addition, to reduce impedance and minimize modulus mismatch between the recording device and the organoid, conducting polymer coatings like poly(3,4-ethylenedioxythiophene) polystyrene sulfonate (PEDOT:PSS)^[51] have been used. A common disadvantage of most electrode materials is their optical opaqueness, which makes them unsuitable for optical imaging techniques such as live-cell imaging.^[38a] For that reason, the use of transparent electrode materials is more advantageous. In this context, a parylene/graphene heterostructure has been applied to stimulate and record electric signals from rat hippocampal neuron assemblies, thanks to the high conductivity, flexibility, and optical transparency of graphene.^[61a] Further works showed the incorporation of both conventional metal electrode feedlines and graphene-based field effect transistors to analyze the electrophysiology of cardiac spheroids.^[38c] An advantage of their approach is the superior spatiotemporal resolution achieved by the high number of electrodes in a single tube.

In addition to graphene, other single-layer materials have been integrated into self-folding devices. One example is MoS₂, which potentially allows for optoelectronic stimulation of cells in vitro (Figure 4F).^[71] Another desired feature of cell analysis platforms is non-perturbative bioanalytical sensing in vitro, which can be achieved through surface-enhanced Raman spectroscopy (SERS). This has been achieved by Gracias and coworkers by functionalizing the inner surface of micro-grippers with plasmonic Au nanostars.^[34a] Silver nanoparticles are another possible candidate for optical probes.^[72] Aptamer-functionalized capacitive biosensors may be a promising technology to introduce the sensing capabilities of small molecules, proteins, and cells into self-folding devices.^[73] For the case of cardiac tissues, incorporating piezoresistive components such as carbon black and crack sensors into tissue analysis platforms may facilitate a direct measurement of the mechanical contractility, which is crucial for investigating drug-induced cardiac toxicity in vitro.^[74] Future devices are expected to provide a combination of multiple functionalities. Pioneering work from Rogers and coworkers demonstrated a multifunctional platform with integrated optical, electrical, chemical, and thermal sensors to precisely monitor the behavior of cortical spheroids.^[54] The simultaneous monitoring

of all these physiological parameters directly from the organoid or tissue in question provides essential data for feeding future computational disease and developmental models.

2.4. Feature Size and Sample Type

Further essential properties of the self-folding devices, in addition to the materials, are shape and size. These properties must be carefully optimized based on the study objective and biological sample of interest. The correlation between the size magnitude and specific application can be visualized in Figure 5A. Lithography-based fabrication provides the advantage of adjusting the feature size since the 3D shape and folding angle can be easily controlled by 2D patterning and film thickness, respectively. Theoretical models provide valuable tools for predicting the morphology based on the geometry and material properties of thin films. A well-established model to predict the curvature radius of rolled-up bilayer tubes is Timoshenko's bimorph beam theory.^[75] Even though this model was developed for bimetallic thermostats, it can also be extended for other materials such as polymeric films,^[34d,37a,45c,76] and is given as

$$\rho = \frac{d[3(1+m)^2 + (1+mn)\{m^2 + (mn)^{-1}\}]}{6\epsilon(1+m)^2} \quad (1)$$

where $d = d_1 + d_2$ is the total thickness of the bilayer, $m = d_1/d_2$ is the ratio of the bilayer thicknesses, $n = Y_1/Y_2$ is the relative elastic modulus, and ϵ is the in-plane biaxial strain between the two layers. The subscripts "1" and "2" denote the first and the second material layer of the bilayer, respectively. Analogous models exist for predicting the morphology change of other strain-induced structures such as wrinkles and helices.^[77]

Self-folding devices can provide specific mechanical environments for mechanobiology studies.^[78] For example, they can be applied to control neurite outgrowth, which is crucial in wiring the nervous system during development and regeneration following trauma or disease.^[79] Williams and coworkers used micro-rolls of different material combinations to encapsulate individual cortical neuronal axons and control their growth, thus resembling the natural myelin present in the brain.^[38a,41,42] The typical diameter range for unmyelinated cortical axons lies between 0.08 and 0.4 μm .^[80] To encapsulate these axons, the researchers achieved micro-rolls as small as 2.7 μm in diameter (Figure 5B).

Single-cell analysis is important in deciphering cell heterogeneity in tissue and disease diagnostics, as larger samples often do not accurately represent the behavior of individual cells.^[40] While eukaryotic cells normally range between 1 and 100 μm in diameter, most animal cells are around 10–30 μm . For single-cell manipulation and analysis, Schmidt and coworkers studied the effects of spatial confinement on cellular behavior and function of yeast cells in tubes with diameters between 1.5 and 14 μm (Figure 5C).^[59a] Gracias and coworkers developed self-folding untethered micro-grippers with sizes ranging from 10 to 70 μm in length (tip-to-tip when open).^[40] These grippers could be used for 3D optical mapping of intrinsic molecular signatures on the membrane of single adenocarcinoma-derived epithelial (MDA-MB-231) cells.^[34a] Cells with more complex structures

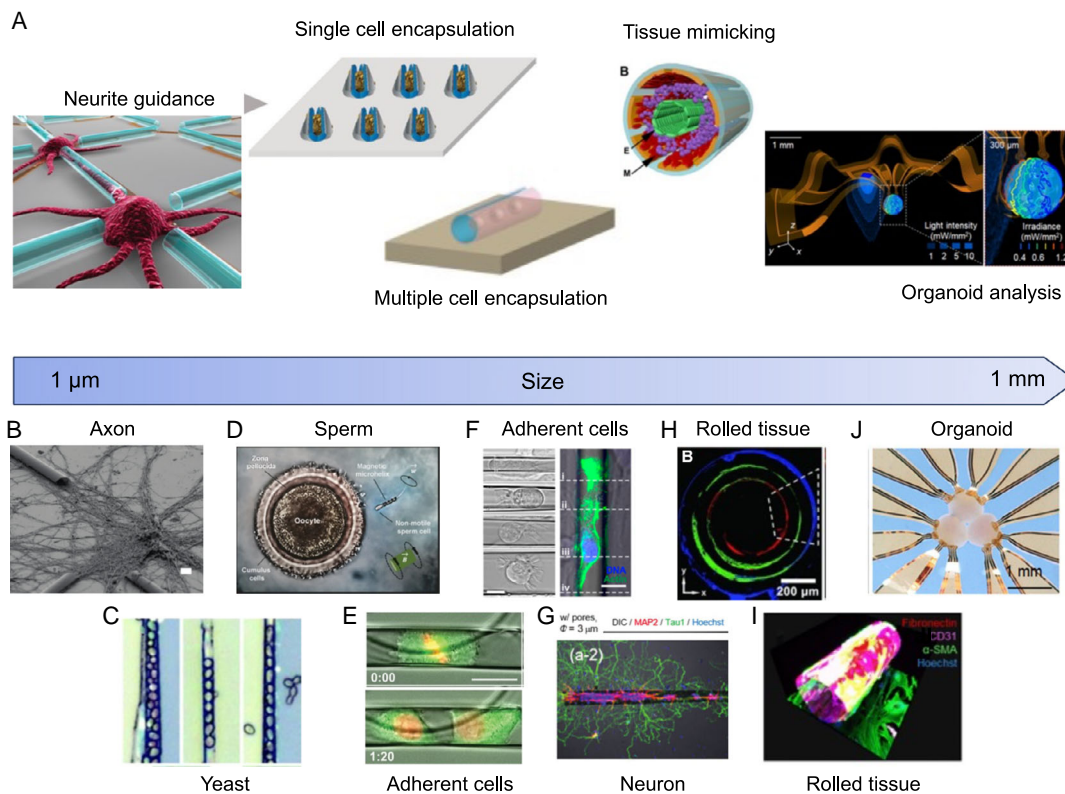


Figure 5. Correlation between the feature size of self-folding devices and their specific purpose, as well as some examples of biological samples with corresponding sizes. A) Different biological applications represented with schematic illustrations ordered by their size scale. B) SEM image of cortical neurons cultured at an intersection of several Si/SiGe tubes in a Si wafer. Scale bar: 10 μm. C) Optical microscope images of yeast cells encapsulated in SiO/SiO₂ microtubes with decreasing diameter from left to right. D) A remotely controlled magnetic helix carrying an immotile sperm and delivering it to the oocyte for fertilization. E) Fluorescent and phase-contrast time-lapse images of a HeLa cell dividing inside a SiO/SiO₂ microtube (Green Fluorescent Protein (GFP)-labelled tubulin, green; H2B-mCherry, red). Scale bar: 15 μm. F) Left: differential interference contrast (DIC) and fluorescence images of a neural stem cell (NSC) trapped inside a SiO/SiO₂ microtube with different diameters. Scale bars: 10 μm. G) Immunocytochemical images of neuron-laden graphene/parylene micro-rolls with 3 μm pores. H) Three cell types cultured in a rolled PDMS membrane, distributed in a fashion similar to blood vessels. Red: endothelial cells (HUVECs); green: smooth muscle cells; blue: fibroblasts (NIH/3T3). I) HUVECs and HUASMCs co-cultured separately on the inner and outer surfaces of a graphene/parylene micro-roll for small-artery mimicking. J) Optical micrographs of a multifunctional pouch-shaped “cage” encapsulating three spheroids in a triangular lattice geometry. (A) Reproduced with permission.^[41] Copyright 2011, American Chemical Society. Reproduced under the terms of the Creative Commons CC BY license.^[34a] Copyright 2017, The Author(s). Published by Wiley-VCH Verlag GmbH & Co. KGaA, Weinheim. Reproduced under the terms of the Creative Commons CC BY license.^[37a] Copyright 2017, The Author(s). Published by Springer Nature Limited. Reproduced under the terms of the Creative Commons CC BY license.^[43b] Copyright 2020, The Author(s). Published by American Association for the Advancement of Science. Reproduced under the terms of the Creative Commons CC BY license.^[54] Copyright 2021, The Author(s). Published by American Association for the Advancement of Science. (B) Reproduced with permission.^[34b] Copyright 2008, Royal Society of Chemistry. (C) Reproduced with permission.^[59a] Copyright 2009, Royal Society of Chemistry. (D) Reproduced with permission.^[65] Copyright 2016, American Chemical Society. (E) Reproduced with permission.^[59c] Copyright 2014, American Chemical Society. (F) Reproduced with permission.^[81] Copyright 2015, American Chemical Society. (G) Adapted with permission.^[45c] Copyright 2023, Royal Society of Chemistry. (H) Reproduced with permission.^[36b] Copyright 2012, WILEY-VCH Verlag GmbH & Co. KGaA, Weinheim. (I) Reproduced with permission.^[45b] Copyright 2023, Royal Society of Chemistry. (J) Reproduced under the terms of the Creative Commons CC BY license.^[54] Copyright 2021, The Author(s). Published by American Association for the Advancement of Science.

such as sperm cells can also be encapsulated and manipulated using devices of a similar size scale. For this case, helical structures (length: $\approx 22 \mu\text{m}$, pitch: $\approx 6 \mu\text{m}$) have proved to be ideal (Figure 5D).^[65] Further studies on single mammalian cells using self-folding devices showed that spatial constraints heavily affected mitotic progression and could cause chromosomal instability (Figure 5E).^[59c] Researchers also demonstrated the correlation between scaffold and migration mode transitions for neural stem cells entering a microtube (Figure 5F).^[81]

The encapsulation of biological samples in the 100 μm range consisting of multiple cells is also relevant. For stem cell culture, 50–600 μm sized wells are optimal for keeping stem cells undifferentiated for long periods without the need for cell passing.^[82] The aggregation of primary rat hippocampal cells and cardiomyocytes were studied using micro-rolls of 50–80 μm diameter. These micro-rolls featured pores whose size was optimized for reagent diffusion and cell-cell communication while keeping cells inside (Figure 5G).^[37a,45c,61a] Micro-rolls of similar

size were also used to investigate neural communications in brain-like 3D cultures.^[61a] The 3D spatiotemporal recording from live cells was achieved using 52–170 μm (tip-to-tip) multi-electrode gripper-shaped shells.^[43a] In addition, the increased size scales allow for the loading of larger samples such as crustacean Triops (tadpole shrimp) embryos and *Artemia* (brine shrimp) eggs.^[34b]

The applications of origami-on-a-chip devices in tissue engineering also necessitate larger sample sizes. One goal is to build engineered tissue *in vitro* to recapitulate the structure and function of tissue *in vivo*. Engineered tissues can range in size from a few hundred micrometers to several millimeters in diameter. The specific size depends on factors such as tissue type, culture duration, and vascularization strategy employed. For example, vascularized neural and liver tissue constructs have been demonstrated at multi-mm³ scales using a synthetic microfluidic vascularization approach.^[83] In contrast, when relying solely on diffusion for oxygen and nutrient supply, tissue constructs are limited to around 100–200 μm.^[84] Self-folding devices provide new strategies for building diverse 3D shapes and incorporating multiple cell types and ECMs. Schmidt and coworkers developed engineered microvasculatures to guide the growth of astrocytes and lumen formation of endothelial cells. These microvasculature constructs were created using porous tubes with varied numbers of windings and hole sizes. The tube diameters in these applications ranged between 15 and 225 μm. The bilayer tubes of SiO and SiO₂ are biodegradable by culturing them in culture medium for five weeks, with the potential for *in vivo* implantation.^[60] Jiang and coworkers patterned human umbilical vein endothelial cells (HUVECs), smooth muscle cells (SMCs), and mouse embryonic fibroblasts (NIH/3T3) in multilayered PDMS tubes with a diameter of 100–2000 μm. This way, they mimicked the physiological assembly of blood vessels and medium-sized veins (Figure 5H).^[36b] The 3D scaffolds of similar size were also used to guide the growth of fibroblasts into different geometries^[38b] and to study the insulin secretion of islet β (β-TC-6) cells.^[50] Gracias and coworkers recapitulated small pulmonary arteries by layering human pulmonary microvascular endothelial cells (HPMECs) and aligned vascular SMCs in microtubes with diameters ranging from 50 to 300 μm.^[43b] Similarly, 20–200 μm diameter micro-rolls were used to mimic the laminar structure of small arteries by co-culturing HUVECs and SMCs across their walls (Figure 5I).^[45b]

Like engineered tissues, organoids can vary significantly in size depending on organ type, culture duration, and growth conditions. While hepatic organoids achieve an average size of 250 μm after 14 days of culture,^[85] brain organoids can reach up to 4 mm in diameter after two months of culture.^[11] It is important to note that organoid size can be highly variable even within the same culture due to the stochastic nature of their development.^[5] Compared to conventional 2D devices, origami-on-a-chip platforms provide a larger contact area, higher signal-to-noise ratio, and a better mechanical stability for encapsulating and analyzing 3D cell assemblies such as organoids and spheroids. In addition, a surface coating to enhance cell attachment is no longer required.^[51] Cohen-Karni and coworkers reported a self-rolled biosensor array to study cell-cell communication within stem-cell-derived cardiac spheroids.^[38c] The inner diameter of the tubes was in the range of 160 μm. Rogers and his

collaborators used pouch-shaped multisensory “cages” to study the spreading of coordinated bursting events across the surface of ≈500 μm cortical spheroids. They also investigated the processes arising from merging more than two spheroids in a single cage (Figure 5J).^[54] Electrophysiological recordings of brain organoids ranging from 400 to 600 μm were carried out using SU-8-based grippers with integrated electrodes by Gracias and coworkers.^[51] They demonstrated that the recordings from 3D shell electrodes were more sensitive to glutamate stimulation compared to traditional 2D electrodes.

3. Future Perspectives

In the last decades, self-folding devices have provided novel cell analysis, tissue engineering, and organoid analysis strategies. Encouraging studies demonstrated the potential of the development of novel multifunctional biointerfaces for 3D cell culture with increasingly complex features.^[54,86] For tissue engineering, self-folding devices could guide cell growth to achieve more complicated structures, such as ventricles. The self-foldable abiotic interface with the cells can mimic the spatial, temporal, and chemical dynamics thanks to their surface sufficiently coated with ECM. Therefore, ideally, the synthetic materials used in self-foldable interfaces should be replaced with natural polymers or ECM itself via newly developed manufacturing methods.^[87] This is critical because not only the microscale scaffold but also the boundary conditions at the nanometer-scale trigger cellular function based on connections between the ECM and mechanotransduction proteins such as integrins. Only then, a cell can find a nanometer cue that it binds with, organize the cytoskeleton appropriately, and transduce micron-scale nonspecific mechanical cues (e.g., osmotic pressures).^[88] This will be crucial in mimicking the structure and function of tissue *in vivo*. One limitation in achieving enhanced complexity is the lack of diffusion, such as vasculature, in current cell culture technologies.^[89] Integration of microfluidic perfusion systems could be beneficial to support scalable and durable culturing.^[90]

As the complexity of input and output systems for stimulation and recording increases, more opportunities are opened to study the behavior of two or more organoids simultaneously. This can be done, for example, by connecting a cardiac organoid and a brain organoid, either via electrodes or directly. Such a system could simulate the electrophysiological response of the human heart to neuronal stimulations and vice versa. Networks of organoids could be interconnected to implement more complex systems, so-called human-on-chips. Current studies showed a combination of two different organoids into a single chip, such as heart and liver^[91] and heart and kidney.^[92] Studies also demonstrated the inclusion of multiple humanized constructs into a single platform, including liver, cardiac, lung, endothelium, brain, and testes organoids.^[93] We believe that multifunctional self-folding devices will be crucial for studying emerging human-on-chip platforms while simultaneously facilitating the interaction between the single constructs via integrated sensors and actuators.

Origami-on-a-chip interfaces with both organoids and engineered tissues could improve the treatment of developmental and degenerative diseases. Tissues derived from patients' cells

could be used to predict patient-specific therapeutic responses. Compared to clinical tests, in vitro disease modeling allows for the direct recording of many more physiological parameters. One example is cardiac contractility, which needs to be monitored during drug therapies. Conventionally, physicians use the end-systolic elastance as the key indicator of cardiac contractility, whose estimation represents a challenge from the clinical perspective.^[94] On the contrary, plenty of approaches have been reported for cardiac contractility monitoring during in vitro drug therapy tests through the integration of mechanical sensors into the tissue culture platforms.^[95] However, current drug screening using patient-derived tissues can take months,^[96] and there is a high demand for efficient methods for timely decisions. For this reason, it is imperative to develop computational models using the data obtained from in vitro assays. A large biological databank combined with state-of-the-art artificial intelligence could further advance the development of the “bio digital twin,” a technology that utilizes software models to replicate the human body and predict diseases. This digital technology could allow therapeutics testing in a quicker, safer, and cost-efficient manner compared to clinical or lab-based tests.

The combination of origami-on-a-chip with organoids could improve the knowledge of human physiology. Human brain organoids could help to enhance the physiological understanding of cognition, learning, and memory. For example, the human brain is more efficient in decision-making and energy consumption compared to computers.^[97] Brain organoids interfaced with computers via complex input–output networks represent an excellent candidate for investigating human and machine intelligence. This “organoid intelligence” field holds the potential to improve the learning and decision-making capabilities of current artificial intelligence models.

4. Conclusions

In this work, we reviewed the development of origami-on-a-chip for interfacing with multi-scale biological samples, including neurites, single cells, and organoids. We focused on the selection of materials, as they are essential in the device’s properties and functionalities. We also highlighted their important contributions to cell analysis and tissue engineering. We anticipate that this technology will help bring cell culture technology closer to replicating and investigating human development and diseases in vitro by providing functional biointerfaces and tissue guiding scaffolds. Combined with advances in biocomputing, these platforms could have a significant impact on the medicine of the future, allowing faster and more advanced computational models to provide patient-specific diagnoses and therapies.

Conflict of Interest

The authors declare no conflict of interest.

Author Contributions

All authors listed have made a substantial, direct, and intellectual contribution to the work and approved it for publication.

Keywords

cell encapsulations, organ on chips, organoids, self-foldings, tissue engineering

Received: January 20, 2024

Revised: May 20, 2024

Published online: June 19, 2024

- [1] C. B. Collin, T. Gebhardt, M. Golebiewski, T. Karaderi, M. Hillemanns, F. M. Khan, A. Salehzadeh-Yazdi, M. Kirschner, S. Krobitch, C. Eu-Stands Pm, L. Kuepfer, *J. Pers. Med.* **2022**, *12*, 166.
- [2] F. Pappalardo, G. Russo, M. Pennisi, G. A. Parasiliti Palumbo, G. Sgroi, S. Motta, D. Maimone, *Cells* **2020**, *9*, 586.
- [3] G. Cosoli, L. Antognoli, L. Scalise, *MethodsX* **2023**, *10*, 102038.
- [4] C. Corro, L. Novellademunt, V. S. W. Li, *Am. J. Physiol. Cell Physiol.* **2020**, *319*, 151.
- [5] Z. Zhao, X. Chen, A. M. Dowbaj, A. Sljukic, K. Bratlie, L. Lin, E. L. S. Fong, G. M. Balachander, Z. Chen, A. Soragni, M. Huch, Y. A. Zeng, Q. Wang, H. Yu, *Nat. Rev. Methods Primers* **2022**, *2*, 94.
- [6] K. Takahashi, K. Tanabe, M. Ohnuki, M. Narita, T. Ichisaka, K. Tomoda, S. Yamanaka, *Cell* **2007**, *131*, 861.
- [7] M. Eiraku, K. Watanabe, M. Matsuo-Takasaki, M. Kawada, S. Yonemura, M. Matsumura, T. Wataya, A. Nishiyama, K. Muguruma, Y. Sasai, *Cell Stem Cell* **2008**, *3*, 519.
- [8] a) G. Berkers, P. van Mourik, A. M. Vonk, E. Kruisselbrink, J. F. Dekkers, K. M. de Winter-de Groot, H. G. M. Arets, R. E. P. Marck-van der Wilt, J. S. Dijkema, M. M. Vanderschuren, R. H. J. Houwen, H. G. M. Heijerman, E. A. van de Graaf, S. G. Elias, C. J. Majoor, G. H. Koppelman, J. Roukema, M. Bakker, H. M. Janssens, R. van der Meer, R. G. J. Vries, H. C. Clevers, H. R. de Jonge, J. M. Beekman, C. K. van der Ent, *Cell Rep.* **2019**, *26*, 1701; b) J. F. Dekkers, C. L. Wiegerinck, H. R. de Jonge, I. Bronsveld, H. M. Janssens, K. M. de Winter-de Groot, A. M. Brandsma, N. W. de Jong, M. J. Bijvelds, B. J. Scholte, E. E. Nieuwenhuis, S. van den Brink, H. Clevers, C. K. van der Ent, S. Middendorp, J. M. Beekman, *Nat. Med.* **2013**, *19*, 939; c) G. Schwank, B. K. Koo, V. Sasselli, J. F. Dekkers, I. Heo, T. Demircan, N. Sasaki, S. Boymans, E. Cuppen, C. K. van der Ent, E. E. Nieuwenhuis, J. M. Beekman, H. Clevers, *Cell Stem Cell* **2013**, *13*, 653.
- [9] A. E. Bigorgne, H. F. Farin, R. Lemoine, N. Mahlaoui, N. Lambert, M. Gil, A. Schulz, P. Philippet, P. Schlessler, T. G. Abrahamson, K. Oymar, E. G. Davies, C. L. Ellingsen, E. Leteurtre, B. Moreau-Massart, D. Berrebi, C. Bole-Feynot, P. Nischke, N. Brousse, A. Fischer, H. Clevers, G. de Saint Basile, *J. Clin. Invest.* **2014**, *124*, 328.
- [10] M. Huch, H. Gehart, R. van Bortel, K. Hamer, F. Blokzijl, M. M. Versteegen, E. Ellis, M. van Wenum, S. A. Fuchs, J. de Ligt, M. van de Wetering, N. Sasaki, S. J. Boers, H. Kemperman, J. de Jonge, J. N. Ijzermans, E. E. Nieuwenhuis, R. Hoekstra, S. Strom, R. R. Vries, L. J. van der Laan, E. Cuppen, H. Clevers, *Cell* **2015**, *160*, 299.
- [11] M. A. Lancaster, M. Renner, C. A. Martin, D. Wenzel, L. S. Bicknell, M. E. Hurles, T. Homfray, J. M. Penninger, A. P. Jackson, J. A. Knoblich, *Nature* **2013**, *501*, 373.
- [12] W. K. Raja, A. E. Mungenast, Y. T. Lin, T. Ko, F. Abdurrob, J. Seo, L. H. Tsai, *PLoS One* **2016**, *11*, 0161969.
- [13] a) H. Kim, H. J. Park, H. Choi, Y. Chang, H. Park, J. Shin, J. Kim, C. J. Lengner, Y. K. Lee, J. Kim, *Stem Cell Rep.* **2019**, *12*, 518; b) L. M. Smits, L. Reinhardt, P. Reinhardt, M. Glatza, A. S. Monzel, N. Stanslowsky, M. D. Rosato-Siri, A. Zanon,

- P. M. Antony, J. Bellmann, S. M. Nicklas, K. Hemmer, X. Qing, E. Berger, N. Kalmbach, M. Ehrlich, S. Bolognin, A. A. Hicks, F. Wegner, J. L. Sternecker, J. C. Schwaborn, *npj Parkinson's Dis.* **2019**, *5*, 5.
- [14] T. Sato, D. E. Stange, M. Ferrante, R. G. Vries, J. H. Van Es, S. Van den Brink, W. J. Van Houdt, A. Pronk, J. Van Gorp, P. D. Siersema, H. Clevers, *Gastroenterology* **2011**, *141*, 1762.
- [15] L. Broutier, G. Mastrogianni, M. M. Versteegen, H. E. Francies, L. M. Gavarro, C. R. Bradshaw, G. E. Allen, R. Arnes-Benito, O. Sidorova, M. P. Gaspersz, N. Georgakopoulos, B. K. Koo, S. Dietmann, S. E. Davies, R. K. Praseedom, R. Lieshout, J. N. M. Iljermans, S. J. Wigmore, K. Saeb-Parsy, M. J. Garnett, L. J. van der Laan, M. Huch, *Nat. Med.* **2017**, *23*, 1424.
- [16] N. Sachs, J. de Ligt, O. Kopper, E. Gogola, G. Bounova, F. Weeber, A. V. Balgobind, K. Wind, A. Gracanin, H. Begthel, J. Korving, R. van Bostel, A. A. Duarte, D. Lelieveld, A. van Hoeck, R. F. Ernst, F. Blokzijl, I. J. Nijman, M. Hoogstraat, M. van de Ven, D. A. Egan, V. Zinzalla, J. Moll, S. F. Boj, E. E. Voest, L. Wessels, P. J. van Diest, S. Rottenberg, R. G. J. Vries, E. Cuppen, et al., *Cell* **2018**, *172*, 373.
- [17] a) G. Wang, M. L. McCain, L. Yang, A. He, F. S. Pasqualini, A. Agarwal, H. Yuan, D. Jiang, D. Zhang, L. Zangi, J. Geva, A. E. Roberts, Q. Ma, J. Ding, J. Chen, D. Z. Wang, K. Li, J. Wang, R. J. Wanders, W. Kulik, F. M. Vaz, M. A. Laflamme, C. E. Murry, K. R. Chien, R. I. Kelley, G. M. Church, K. K. Parker, W. T. Pu, *Nat. Med.* **2014**, *20*, 616; b) S. J. Park, D. Zhang, Y. Qi, Y. Li, K. Y. Lee, V. J. Bezzerides, P. Yang, S. Xia, S. L. Kim, X. Liu, F. Lu, F. S. Pasqualini, P. H. Campbell, J. Geva, A. E. Roberts, A. G. Kleber, D. J. Abrams, W. T. Pu, K. K. Parker, *Circulation* **2019**, *140*, 390; c) S. L. Kim, M. A. Trembley, K. Y. Lee, S. Choi, L. A. MacQueen, J. F. Zimmerman, L. H. C. de Wit, K. Shani, D. E. Henze, D. J. Drennan, S. A. Saifee, L. J. Loh, X. Liu, K. K. Parker, W. T. Pu, *Stem Cell Rep.* **2023**, *18*, 1811; d) Q. Jin, K. Y. Lee, Z. Selimi, D. Shimura, E. Wang, J. F. Zimmerman, R. M. Shaw, J. P. Kucera, K. K. Parker, J. E. Saffitz, A. G. Kleber, *J. Mol. Cell. Cardiol.* **2024**, *186*, 71.
- [18] a) A. P. Nesmith, M. A. Wagner, F. S. Pasqualini, B. B. O'Connor, M. J. Pincus, P. R. August, K. K. Parker, *J. Cell Biol.* **2016**, *215*, 47; b) Z. Al Tanoury, J. F. Zimmerman, J. Rao, D. Sieiro, H. M. McNamara, T. Cherrier, A. Rodriguez-delaRosa, A. Hick-Colin, F. Bousson, C. Fugier-Schmucker, F. Marchiano, B. Habermann, J. Chal, A. P. Nesmith, S. Gapon, E. Wagner, V. A. Gupta, R. Bassel-Duby, E. N. Olson, A. E. Cohen, K. K. Parker, O. Pourquie, *Proc. Natl. Acad. Sci.* **2021**, *118*, e2022960118.
- [19] a) K. H. Benam, S. Dauth, B. Hassell, A. Herland, A. Jain, K. J. Jang, K. Karalis, H. J. Kim, L. MacQueen, R. Mahmoodian, S. Musah, Y. S. Torisawa, A. D. van der Meer, R. Villenave, M. Yadid, K. K. Parker, D. E. Ingber, *Annu. Rev. Pathol.: Mech. Dis.* **2015**, *10*, 195; b) J. Cable, P. Arlotta, K. K. Parker, A. J. Hughes, K. Goodwin, C. L. Mummery, R. D. Kamm, S. J. Engle, D. A. Tagle, S. F. Boj, A. E. Stanton, Y. Morishita, M. L. Kemp, D. A. Norfleet, E. E. May, A. Lu, R. Bashir, A. W. Feinberg, S. M. Hull, A. L. Gonzalez, M. R. Blatchley, N. Montserrat Pulido, R. Morizane, T. C. McDevitt, D. Mishra, A. Mulero-Russe, *Ann. N. Y. Acad. Sci.* **2022**, *1518*, 183.
- [20] J. Haft, *Prog. Cardiovasc. Dis.* **1974**, *16*, 539.
- [21] R. L. Ploesteanu, A. C. Nechita, D. Turcu, B. N. Manolescu, S. C. Stamate, M. Berteau, *J. Med. Life* **2018**, *11*, 107.
- [22] a) C. Nappia, L. Zappia, G. Laterra, M. Roberto, *Ann. Noninvasive Electrocardiol.* **2020**, *25*, e12726; b) M. A. Marinella, *Am. Fam. Physician* **1998**, *57*, 699.
- [23] V. Eapen, R. Baker, A. Walter, V. Raghupathy, J. J. Wehrman, P. F. Sowman, *Brain Sci.* **2017**, *7*, 161.
- [24] R. S. Fisher, A. L. Velasco, *Nat. Rev. Neurol.* **2014**, *10*, 261.
- [25] E. Tanovic, *Bosnian J. Basic Med. Sci.* **2009**, *9*, 49.
- [26] L. Xu, S. R. Gutbrod, A. P. Bonifas, Y. Su, M. S. Sulkin, N. Lu, H.-J. Chung, K.-I. Jang, Z. Liu, M. Ying, C. Lu, R. C. Webb, J.-S. Kim, J. I. Laughner, H. Cheng, Y. Liu, A. Ameen, J.-W. Jeong, G.-T. Kim, Y. Huang, I. R. Efimov, J. A. Rogers, *Nat. Commun.* **2014**, *5*, 3329.
- [27] J. Icha, M. Weber, J. C. Waters, C. Norden, *Bioessays* **2017**, *39*, 1700003.
- [28] a) L. Grob, P. Rinklin, S. Zips, D. Mayer, S. Weidlich, K. Terkan, L. J. K. Weiss, N. Adly, A. Offenhausser, B. Wolfrum, *Sensors* **2021**, *21*, 3981; b) H. Peng, L. Grob, L. J. K. Weiss, L. Hiendlmeier, E. Music, I. Kopic, T. F. Teshima, P. Rinklin, B. Wolfrum, *Nanoscale* **2023**, *15*, 4006; c) S. Zips, L. Grob, P. Rinklin, K. Terkan, N. Y. Adly, L. J. K. Weiss, D. Mayer, B. Wolfrum, *ACS Appl. Mater. Interfaces* **2019**, *11*, 32778.
- [29] M. S. Saleh, S. M. Ritchie, M. A. Nicholas, H. L. Gordon, C. Hu, S. Jahan, B. Yuan, R. Bezbaruah, J. W. Reddy, Z. Ahmed, M. Chamanzar, E. A. Yttri, R. P. Panat, *Sci. Adv.* **2022**, *8*, eabj4853.
- [30] a) S. Chen, J. Chen, X. Zhang, Z. Y. Li, J. Li, *Light: Sci. Appl.* **2020**, *9*, 75; b) R. Fernandes, D. H. Gracias, *Adv. Drug Delivery Rev.* **2012**, *64*, 1579; c) L. Ionov, *Soft Matter* **2011**, *7*, 6786; d) T. G. Leong, A. M. Zarfshar, D. H. Gracias, *Small* **2010**, *6*, 792; e) J. Rogers, Y. Huang, O. G. Schmidt, D. H. Gracias, *MRS Bull.* **2016**, *41*, 123.
- [31] Q. Lyu, S. Gong, J. G. Lees, J. Yin, L. W. Yap, A. M. Kong, Q. Shi, R. Fu, Q. Zhu, A. Dyer, J. M. Dyson, S. Y. Lim, W. Cheng, *Nat. Commun.* **2022**, *13*, 7259.
- [32] a) V. Y. Prinz, V. A. Seleznev, A. K. Gutakovskiy, A. V. Chehovskiy, V. V. Preobrazhenskii, M. A. Putyato, T. A. Gavrilova, *Phys. E* **2000**, *6*, 828; b) O. G. Schmidt, K. Eberl, *Nature* **2001**, *410*, 168.
- [33] S. Choi, K. Y. Lee, S. L. Kim, L. A. MacQueen, H. Chang, J. F. Zimmerman, Q. Jin, M. M. Peters, H. A. M. Ardon, X. Liu, A. C. Heiler, R. Gabardi, C. Richardson, W. T. Pu, A. R. Bausch, K. K. Parker, *Nat. Mater.* **2023**, *22*, 1039.
- [34] a) Q. Jin, M. Li, B. Polat, S. K. Paidi, A. Dai, A. Zhang, J. V. Pagaduan, I. Barman, D. H. Gracias, *Angew. Chem., Int. Ed. Engl.* **2017**, *56*, 3822; b) T. G. Leong, C. L. Randall, B. R. Benson, A. M. Zarfshar, D. H. Gracias, *Lab Chip* **2008**, *8*, 1621; c) G. Stoychev, N. Pureskiy, L. Ionov, *Soft Matter* **2011**, *7*, 3277; d) V. Stroganov, M. Al-Hussein, J. U. Sommer, A. Janke, S. Zakharchenko, L. Ionov, *Nano Lett.* **2015**, *15*, 1786; e) V. Stroganov, S. Zakharchenko, E. Sperling, A. K. Meyer, O. G. Schmidt, L. Ionov, *Adv. Funct. Mater.* **2014**, *24*, 4357; f) W. Xu, Z. Qin, C. T. Chen, H. R. Kwag, Q. Ma, A. Sarkar, M. J. Buehler, D. H. Gracias, *Sci. Adv.* **2017**, *3*, 1701084.
- [35] M. Ha, G. S. Canon Bermudez, J. A. Liu, E. S. Oliveros Mata, B. A. Evans, J. B. Tracy, D. Makarov, *Adv. Mater.* **2021**, *33*, 2008751.
- [36] a) F. Cavallo, Y. Huang, E. W. Dent, J. C. Williams, M. G. Lagally, *ACS Nano* **2014**, *8*, 12219; b) B. Yuan, Y. Jin, Y. Sun, D. Wang, J. Sun, Z. Wang, W. Zhang, X. Jiang, *Adv. Mater.* **2012**, *24*, 890.
- [37] a) T. F. Teshima, H. Nakashima, Y. Ueno, S. Sasaki, C. S. Henderson, S. Tsukada, *Sci. Rep.* **2017**, *7*, 17376; b) S. Zakharchenko, N. Pureskiy, G. Stoychev, M. Stamm, L. Ionov, *Soft Matter* **2010**, *6*, 2633; c) S. Zakharchenko, N. Pureskiy, G. Stoychev, C. Waurisch, S. G. Hickey, A. Eychmuller, J. U. Sommer, L. Ionov, *J. Mater. Chem. B* **2013**, *1*, 1786.
- [38] a) P. Froeter, Y. Huang, O. V. Cangellaris, W. Huang, E. W. Dent, M. U. Gillette, J. C. Williams, X. Li, *ACS Nano* **2014**, *8*, 11108; b) M. Jamal, N. Bassik, J. H. Cho, C. L. Randall, D. H. Gracias, *Biomaterials* **2010**, *31*, 1683; c) A. Kalmykov, C. Huang, J. Bliley, D. Shiwerski, J. Tashman, A. Abdullah, S. K. Rastogi, S. Shukla, E. Mataev, A. W. Feinberg, K. J. Hsia, T. Cohen-Karni, *Sci. Adv.* **2019**, *5*, eaax0729.
- [39] L. Mahadevan, S. Rica, *Science* **2005**, *307*, 1740.

- [40] K. Malachowski, M. Jamal, Q. Jin, B. Polat, C. J. Morris, D. H. Gracias, *Nano Lett.* **2014**, *14*, 4164.
- [41] M. Yu, Y. Huang, J. Ballweg, H. Shin, M. Huang, D. E. Savage, M. G. Lagally, E. W. Dent, R. H. Blick, J. C. Williams, *ACS Nano* **2011**, *5*, 2447.
- [42] C. S. Bausch, A. Koitmäe, E. Stava, A. Price, P. J. Resto, Y. Huang, D. Sonnenberg, Y. Stark, C. Heyn, J. C. Williams, E. W. Dent, R. H. Blick, *Appl. Phys. Lett.* **2013**, *103*, 173705.
- [43] a) J. Cools, Q. Jin, E. Yoon, D. Alba Burbano, Z. Luo, D. Cuypers, G. Callewaert, D. Braeken, D. H. Gracias, *Adv. Sci.* **2018**, *5*, 1700731; b) Q. Jin, A. Bhatta, J. V. Pagaduan, X. Chen, H. West-Foyle, J. Liu, A. Hou, D. Berkowitz, S. C. Kuo, F. B. Askin, T. D. Nguyen, D. H. Gracias, L. H. Romer, *Sci. Adv.* **2020**, *6*, eaaz2598.
- [44] S. Dabral, J. Van Etten, X. Zhang, C. Apblett, G. R. Yang, P. Ficalora, J. F. McDonald, *J. Electron. Mater.* **1992**, *21*, 989.
- [45] a) T. Goto, T. F. Teshima, K. Sakai, M. Yamaguchi, *AIP Adv.* **2022**, *12*, 075002; b) K. Sakai, S. Miura, T. F. Teshima, T. Goto, S. Takeuchi, M. Yamaguchi, *Nanoscale Horiz.* **2023**, *8*, 1529; c) K. Sakai, T. F. Teshima, H. Nakashima, Y. Ueno, *Nanoscale* **2019**, *11*, 13249; d) T. F. Teshima, C. S. Henderson, M. Takamura, Y. Ogawa, S. Wang, Y. Kashimura, S. Sasaki, T. Goto, H. Nakashima, Y. Ueno, *Nano Lett.* **2019**, *19*, 461.
- [46] T. G. Leong, B. R. Benson, E. K. Call, D. H. Gracias, *Small* **2008**, *4*, 1605.
- [47] K. Kobayashi, C. Yoon, S. H. Oh, J. V. Pagaduan, D. H. Gracias, *ACS Appl. Mater. Interfaces* **2019**, *11*, 151.
- [48] Q. Jin, Y. Yang, J. A. Jackson, C. Yoon, D. H. Gracias, *Nano Lett.* **2020**, *20*, 5383.
- [49] S. Zakharchenko, E. Sperling, L. Ionov, *Biomacromolecules* **2011**, *12*, 2211.
- [50] M. Jamal, S. S. Kadam, R. Xiao, F. Jivan, T. M. Onn, R. Fernandes, T. D. Nguyen, D. H. Gracias, *Adv. Healthcare Mater.* **2013**, *2*, 1142.
- [51] Q. Huang, B. Tang, J. C. Romero, Y. Yang, S. K. Elsayed, G. Pahapale, T. J. Lee, I. E. Morales Pantoja, F. Han, C. Berlinicke, T. Xiang, M. Solazzo, T. Hartung, Z. Qin, B. S. Caffo, L. Smirnova, D. H. Gracias, *Sci. Adv.* **2022**, *8*, eabq5031.
- [52] Q. Huang, T. Deng, W. Xu, C. Yoon, Z. Qin, Y. Lin, T. Li, Y. Yang, M. Shen, S. M. Thon, J. B. Khurgin, D. H. Gracias, *Adv. Intell. Syst.* **2023**, *5*, 2000195.
- [53] F. Cavallo, K. T. Turner, M. G. Lagally, *Adv. Funct. Mater.* **2014**, *24*, 1730.
- [54] Y. Park, C. K. Franz, H. Ryu, H. Luan, K. Y. Cotton, J. U. Kim, T. S. Chung, S. Zhao, A. Vazquez-Guardado, D. S. Yang, K. Li, R. Avila, J. K. Phillips, M. J. Quezada, H. Jang, S. S. Kwak, S. M. Won, K. Kwon, H. Jeong, A. J. Bandodkar, M. Han, H. Zhao, G. R. Osher, H. Wang, K. Lee, Y. Zhang, Y. Huang, J. D. Finan, J. A. Rogers, *Sci. Adv.* **2021**, *7*, eabf9153.
- [55] K. Kuribayashi-Shigetomi, H. Onoe, S. Takeuchi, *PLoS One* **2012**, *7*, e51085.
- [56] A. J. Hughes, H. Miyazaki, M. C. Coyle, J. Zhang, M. T. Laurie, D. Chu, Z. Vavrusova, R. A. Schneider, O. D. Klein, Z. J. Gartner, *Dev. Cell* **2018**, *44*, 165.
- [57] K. A. W. Feinberg, A. Feigel, S. S. Shevkopyas, S. Sheehy, G. M. Whitesides, K. K. Parker, *Science* **2007**, *317*, 1366.
- [58] A. W. Feinberg, K. K. Parker, *Nano Lett.* **2010**, *10*, 2184.
- [59] a) G. Huang, Y. Mei, D. J. Thurmer, E. Coric, O. G. Schmidt, *Lab Chip* **2009**, *9*, 263; b) E. J. Smith, S. Schulze, S. Kiravittaya, Y. Mei, S. Sanchez, O. G. Schmidt, *Nano Lett.* **2011**, *11*, 4037; c) W. Xi, C. K. Schmidt, S. Sanchez, D. H. Gracias, R. E. Carazo-Salas, S. P. Jackson, O. G. Schmidt, *Nano Lett.* **2014**, *14*, 4197.
- [60] R. Arayanarokool, A. K. Meyer, L. Helbig, S. Sanchez, O. G. Schmidt, *Lab Chip* **2015**, *15*, 2981.
- [61] a) K. Sakai, T. F. Teshima, T. Goto, H. Nakashima, M. Yamaguchi, *Adv. Funct. Mater.* **2023**, *33*, 2301836; b) T. Teshima, H. Onoe, H. Aonuma, K. Kuribayashi-Shigetomi, K. Kamiya, T. Tonooka, H. Kanuka, S. Takeuchi, *Adv. Mater.* **2014**, *26*, 2850; c) T. Teshima, H. Onoe, K. Kuribayashi-Shigetomi, H. Aonuma, K. Kamiya, H. Ishihara, H. Kanuka, S. Takeuchi, *Small* **2014**, *10*, 912.
- [62] K. E. Laflin, C. J. Morris, T. Muqeem, D. H. Gracias, *Appl. Phys. Lett.* **2012**, *101*, 131901.
- [63] a) G. Huang, V. A. Bolanos Quinones, F. Ding, S. Kiravittaya, Y. Mei, O. G. Schmidt, *ACS Nano* **2010**, *4*, 3123; b) G. S. Huang, S. Kiravittaya, V. A. Bolaños Quiñones, F. Ding, M. Benyoucef, A. Rastelli, Y. F. Mei, O. G. Schmidt, *Appl. Phys. Lett.* **2009**, *94*, 141901.
- [64] V. Magdanz, S. Sanchez, O. G. Schmidt, *Adv. Mater.* **2013**, *25*, 6581.
- [65] M. Medina-Sanchez, L. Schwarz, A. K. Meyer, F. Hebenstreit, O. G. Schmidt, *Nano Lett.* **2016**, *16*, 555.
- [66] a) O. Mastikhina, B.-U. Moon, K. Williams, R. Hatkar, D. Gustafson, O. Mourad, X. Sun, M. Koo, A. Y. L. Lam, Y. Sun, J. E. Fish, E. W. K. Young, S. S. Nunes, *Biomaterials* **2020**, *233*, 119741; b) F. Zhang, K.-Y. Qu, B. Zhou, Y. Luo, Z. Zhu, D.-J. Pan, C. Cui, Y. Zhu, M.-L. Chen, N.-P. Huang, *Biosens. Bioelectron.* **2021**, *179*, 113080; c) Y. Zhao, N. Rafatian, N. T. Feric, B. J. Cox, R. Aschar-Sobbi, E. Y. Wang, P. Aggarwal, B. Zhang, G. Conant, K. Ronaldson-Bouchard, A. Pahnke, S. Protze, J. H. Lee, L. Davenport Huyer, D. Jekic, A. Wickeler, H. E. Naguib, G. M. Keller, G. Vunjak-Novakovic, U. Broeckel, P. H. Backx, M. Radisic, *Cell* **2019**, *176*, 913.
- [67] a) L. Hiendlmeier, F. Zurita, J. Vogel, F. Del Duca, G. Al Boustani, H. Peng, I. Kopic, M. Nikić, T. F. Teshima, B. Wolfrum, *Adv. Mater.* **2023**, *35*, 2210206; b) Z. Jiang, N. Chen, Z. Yi, J. Zhong, F. Zhang, S. Ji, R. Liao, Y. Wang, H. Li, Z. Liu, Y. Wang, T. Yokota, X. Liu, K. Fukuda, X. Chen, T. Someya, *Nat. Electron.* **2022**, *5*, 784; c) S. Lacour, D. Chan, S. Wagner, T. Li, Z. Suo, *Appl. Phys. Lett.* **2006**, *88*, 204103.
- [68] a) V. Emmenegger, M. E. J. Obien, F. Franke, A. Hierlemann, *Front. Cell. Neurosci.* **2019**, *13*, 159; b) R. Hinch, *Prog. Biophys. Mol. Biol.* **2002**, *78*, 45.
- [69] X. Yang, C. Forró, T. L. Li, Y. Miura, T. J. Zaluska, C.-T. Tsai, S. Kanton, J. P. McQueen, X. Chen, V. Mollo, F. Santoro, S. P. Paşca, B. Cui, *Nat. Biotechnol.* **2024**, <https://doi.org/10.1101/2023.09.22.5590502023.09.22.559050>
- [70] C. M. Tringides, N. Vachicouras, I. de Lazaro, H. Wang, A. Trouillet, B. R. Seo, A. Elosegui-Artola, F. Fallegger, Y. Shin, C. Casiraghi, K. Kostarelos, S. P. Lacour, D. J. Mooney, *Nat. Nanotechnol.* **2021**, *16*, 1019.
- [71] W. Xu, T. Li, Z. Qin, Q. Huang, H. Gao, K. Kang, J. Park, M. J. Buehler, J. B. Khurgin, D. H. Gracias, *Nano Lett.* **2019**, *19*, 7941.
- [72] H. Marks, M. Schechinger, J. Garza, A. Locke, G. Coté, *Nanophotonics* **2017**, *6*, 681.
- [73] S. Weaver, M. H. Mohammadi, N. Nakatsuka, *Biosens. Bioelectron.* **2023**, *224*, 115014.
- [74] a) W. Dou, M. Malhi, T. Cui, M. Wang, T. Wang, G. Shan, J. Law, Z. Gong, J. Plakhotnik, T. Filleter, R. Li, C. A. Simmons, J. T. Maynes, Y. Sun, *ACS Nano* **2022**, *16*, 11278; b) D.-S. Kim, Y. W. Choi, A. Shanmugasundaram, Y.-J. Jeong, J. Park, N.-E. Oyunbaatar, E.-S. Kim, M. Choi, D.-W. Lee, *Nat. Commun.* **2020**, *11*, 535; c) J. U. Lind, T. A. Busbee, A. D. Valentine, F. S. Pasqualini, H. Yuan, M. Yadid, S.-J. Park, A. Kotikian, A. P. Nesmith, P. H. Campbell, J. J. Vlassak, J. A. Lewis, K. K. Parker, *Nat. Mater.* **2017**, *16*, 303.
- [75] S. Timoshenko, *J. Opt. Soc. Am.* **1925**, *11*, 233.

- [76] a) R. M. Erb, J. S. Sander, R. Grisch, A. R. Studart, *Nat. Commun.* **2013**, *4*, 1712; b) H.-W. Huang, M. S. Sakar, A. J. Petruska, S. Pané, B. J. Nelson, *Nat. Commun.* **2016**, *7*, 12263.
- [77] Z. Chen, G. Huang, I. Trase, X. Han, Y. Mei, *Phys. Rev. Appl.* **2016**, *5*, 017001.
- [78] J. Männik, T. F. Teshima, B. Wolftrum, D. Yang, *J. Appl. Phys.* **2021**, *129*, 210905.
- [79] E. T. Stoeckli, *Development* **2018**, *145*, 151415.
- [80] D. Debanne, *Nat. Rev. Neurosci.* **2004**, *5*, 304.
- [81] B. Koch, A. K. Meyer, L. Helbig, S. M. Harazim, A. Storch, S. Sanchez, O. G. Schmidt, *Nano Lett.* **2015**, *15*, 5530.
- [82] J. C. Mohr, J. J. de Pablo, S. P. Palecek, *Biomaterials* **2006**, *27*, 6032.
- [83] S. Grebenyuk, A. R. Abdel Fattah, M. Kumar, B. Toprakhisar, G. Rustandi, A. Vananroye, I. Salmon, C. Verfaillie, M. Grillo, A. Ranga, *Nat. Commun.* **2023**, *14*, 193.
- [84] J. Rouwkema, B. F. J. M. Koopman, C. A. V. Blitterswijk, W. J. A. Dhert, J. Malda, *Biotechnol. Genet. Eng. Rev.* **2009**, *26*, 163.
- [85] S. P. Harrison, R. Siller, Y. Tanaka, M. E. Chollet, M. E. de la Morena-Barrio, Y. Xiang, B. Patterson, E. Andersen, C. Bravo-Pérez, H. Kempf, K. S. Åsrud, O. Lunov, A. Dejneka, M.-C. Mowinckel, B. Stavik, P. M. , E. Melum, S. Baumgarten, F. Bonanini, D. Kurek, S. Mathapati, R. Almaas, K. Sharma, S. R. Wilson, F. S. Skottvoll, I. C. Boger, I. L. Bogen, T. A. Nyman, J. J. Wu, A. Bezrouk, et al., *Exp. Mol. Med.* **2023**, *55*, 2005.
- [86] Y. Park, T. S. Chung, J. A. Rogers, *Curr. Opin. Biotechnol.* **2021**, *72*, 1.
- [87] a) J. A. Rowley, G. Madlambayan, D. J. Mooney, *Biomaterials* **1999**, *20*, 45; b) N. Huebsch, P. R. Arany, A. S. Mao, D. Shvartsman, O. A. Ali, S. A. Bencherif, J. Rivera-Feliciano, D. J. Mooney, *Nat. Mater.* **2010**, *9*, 518.
- [88] A. Grosberg, P. L. Kuo, C. L. Guo, N. A. Geisse, M. A. Bray, W. J. Adams, S. P. Sheehy, K. K. Parker, *PLoS Comput. Biol.* **2011**, *7*, 1001088.
- [89] S. Zhang, Z. Wan, R. D. Kamm, *Lab Chip* **2021**, *21*, 473.
- [90] A. Roth, M.-W. Berlin, *Science* **2021**, *373*, 1304.
- [91] F. Yin, X. Zhang, L. Wang, Y. Wang, Y. Zhu, Z. Li, T. Tao, W. Chen, H. Yu, J. Qin, *Lab Chip* **2021**, *21*, 571.
- [92] B. Gabbin, V. Meraviglia, M. L. Angenent, D. Ward-van Oostwaard, W. Sol, C. L. Mummery, T. J. Rabelink, B. J. van Meer, C. W. van den Berg, M. Bellin, *Mater. Today Bio* **2023**, *23*, 100818.
- [93] S. A. P. Rajan, J. Aleman, M. Wan, N. Pourhabibi Zareandi, G. Nzou, S. Murphy, C. E. Bishop, H. Sadri-Ardekani, T. Shupe, A. Atala, A. R. Hall, A. Skardal, *Acta Biomater.* **2020**, *106*, 124.
- [94] Y. Kataoka, Y. Fukuda, I. Shelly, J. Peterson, S. Yokota, K. Uemura, K. Saku, J. Alexander, K. Sunagawa, in *2023 45th Annual Int. Conf. IEEE Engineering in Medicine & Biology Society (EMBC)*, IEEE, Piscataway, NJ **2023**, p. 1.
- [95] W. Dou, M. Malhi, Q. Zhao, L. Wang, Z. Huang, J. Law, N. Liu, C. A. Simmons, J. T. Maynes, Y. Sun, *Microsyst. Nanoeng.* **2022**, *8*, 26.
- [96] C. Calandrini, S. R. van Hooff, I. Paassen, D. Ayyildiz, S. Derakhshan, M. E. M. Dolman, K. P. S. Langenberg, M. van de Ven, C. de Heus, N. Liv, M. Kool, R. R. de Krijger, G. A. M. Tytgat, M. M. van den Heuvel-Eibrink, J. J. Molenaar, J. Drost, *Cell Rep.* **2021**, *36*, 109568.
- [97] a) I. E. Morales Pantoja, L. Smirnova, A. R. Muotri, K. J. Wahlin, J. Kahn, J. L. Boyd, D. H. Gracias, T. D. Harris, T. Cohen-Karni, B. S. Caffo, A. S. Szalay, F. Han, D. J. Zack, R. Etienne-Cummings, A. Akwaboah, J. C. Romero, D.-M. Alam El Din, J. D. Plotkin, B. L. Paulhamus, E. C. Johnson, F. Gilbert, J. L. Curley, B. Cappiello, J. C. Schwamborn, E. J. Hill, P. Roach, D. Tornero, C. Krall, R. Parri, F. Sillé, A. Levchenko, R. E. Jabbour, B. J. Kagan, C. A. Berlinicke, Q. Huang, A. Maertens, K. Herrmann, K. Tsaion, R. Dastgheyb, C. W. Habela, J. T. Vogelstein, T. Hartung, *Front. Artif. Intell.* **2023**, *6*, 1116870; b) L. Smirnova, B. S. Caffo, D. H. Gracias, Q. Huang, I. E. Morales Pantoja, B. Tang, D. J. Zack, C. A. Berlinicke, J. L. Boyd, T. D. Harris, E. C. Johnson, B. J. Kagan, J. Kahn, A. R. Muotri, B. L. Paulhamus, J. C. Schwamborn, J. Plotkin, A. S. Szalay, J. T. Vogelstein, P. F. Worley, T. Hartung, *Front. Sci.* **2023**, *1*, 1017235; c) L. Smirnova, I. E. Morales Pantoja, T. Hartung, *Altex* **2023**, *40*, 191.



Alonso Ingar Romero graduated from the Technical University of Darmstadt with B.D and M.D. degrees in electrical engineering. Due to his passion in the biomedical field, he moved to Technical University of Munich to join the NTT Research-TUM project as a part of his Ph.D. studies. He is currently working on foldable electronics for interfacing 3D cardiac cell aggregates.



Qianru Jin received her B.S. degree in chemical engineering from Tsinghua University, China and her Ph.D. degree in chemical and biomolecular Engineering, from the Johns Hopkins University, USA. From 2018 until 2019, she was a post-doctoral researcher at the Johns Hopkins University. Since 2019, she is a postdoctoral fellow at Harvard John A. Paulson School of Engineering and Applied Sciences, USA. She is involved in the project of identification of cardiac electrical dysfunction and rescue of a severe arrhythmia.



Kevin Kit Parker received his B.S. degree in biomedical engineering from Boston University, his M.S. degree in mechanical engineering and Ph.D. degree in applied physics from Vanderbilt University in 1998. He was a postdoctoral fellow at the Johns Hopkins School of Medicine from 2001 until 2002. After serving on the Defense Science Research Council, he led his Disease Biophysics Group as Tarr Family Professor of Bioengineering and Applied Physics in the School of Engineering and Applied Sciences at Harvard University as well as the faculty member at Boston Children's Hospital, the Harvard Stem Cell Institute, and the Wyss Institute for Biologically Inspired Engineering.



Joe Alexander received B.D. degree in chemical engineering from Auburn University, and both M.D. and Ph.D. degrees in biomedical engineering from Johns Hopkins Medical School. Then, he completed a cardiology research fellowship at Albert Einstein College of Medicine before receiving additional training as a Japan Society for Promotion of Science (JSPS) Fellow at Kyushu University. Later, he held academic faculty positions in biomedical engineering and in medicine at Vanderbilt University while completing a residency in internal medicine at Vanderbilt Hospital. After more than 20 years of experience in the pharmaceutical industry, he is specializing in cardiovascular dynamics as a senior vice president and director of Medical and Health Informatics Laboratory, NTT Research Inc.



Bernhard Wolfrum studied physics in Göttingen and Santa Barbara before obtaining his Ph.D. degree at the University of Göttingen in 2004. He afterward conducted postdoctoral research at the Forschungszentrum Jülich and the University of Delft. From 2009 until 2015, he led a Helmholtz Young Investigator group at Forschungszentrum Jülich. He lectured as a junior professor at RWTH Aachen from 2011 until starting at TUM in 2015. In 2017, he conducted research as a visiting associate professor at Tohoku University in Sendai. His research focuses on neuro- and bioelectronics including electrochemical sensor arrays and interfaces for mapping chemical cues and stimulating signals in cellular networks.



Tetsuhiko F. Teshima received a B.S. degree in veterinary medicine, M.S. degree in cell biology, and his Ph.D. degree in information science and technology from the University of Tokyo, Japan. Since 2014, he was a postdoctoral researcher at NTT Basic Research Laboratories, Japan. In 2020, he started to work as a senior research scientist at NTT Research Inc., USA, a visiting scholar at Technische Universität München, Germany, and the guest international associate professor at Keio University, Japan. He is broadly interested in self-assembly of nanomaterials and soft materials with a particular focus on the bioelectronics and biointerfaces.